Modulation of ISOs by Land-Atmosphere Feedback and Contribution to the Interannual Variability of Indian Summer Monsoon

Subodh Kumar Saha,[1] Subhadeep Halder,[1] A. Suryachandra Rao,[1] B. N. Goswami,[1]

Subodh Kumar Saha, Indian Institute of Tropical Meteorology, Pune 411008, India (subodh@tropmet.res.in)

Subhadeep Halder, Indian Institute of Tropical Meteorology, Pune 411008, India (shalder@tropmet.res.in)

A. Suryachandra Rao, Indian Institute of Tropical Meteorology, Pune 411008, India (surya@tropmet.res.in)

B. N. Goswami, Indian Institute of Tropical Meteorology, Pune 411008, India (goswami@tropmet.res.in)

[1]Indian Institute of Tropical Meteorology,
Dr. Homi Bhabha Road, Pune 411008,
India.

Abstract.

A mechanism of internal variability of Indian summer monsoon through the modulation of intraseasonal oscillation (ISO) by land-atmosphere feedback is proposed. Evidence of feedback between surface soil moisture and ISOs is seen in the soil moisture data from GSWP-2 and rainfall data from observations. Using two sets of internal simulation by a regional climate model (RCM), it is shown that internally generated anomalous soil moisture interacts with the following ISO and generates interannual variability. To gain further insight, 27 years of sensitivity experiment by prescribing wet (dry) soil moisture condition during break (active) period along with a control simulation are carried out. The sensitivity experiment reveals the large-scale nature of soil moisture and ISO feedback which takes place through the changes in atmospheric stability by altering lower-level atmospheric conditions. The feedback is inherent to the monsoon system and a part of it acts through the intraseasonal varying memory of soil moisture. The RCM used to test the hypothesis is constrained by one-way interactions at the lateral boundary. Experiments with a much larger domain upheld the findings and hence suggest the true nature of soil moisture and ISO feedback present in the monsoon system.

1. Introduction

Prediction of Indian summer monsoon rainfall (ISMR) well in advance has immense importance in terms of economy and day-to-day life of the people in this region. However, the predictability of the Indian summer monsoon rainfall is limited by the internal variability. The low frequency component of slowly varying large scale influences (e.g. SST, snow cover etc.) explains only about half of the interannual variability and the remaining part is due to internal dynamics [*Sperber and Palmer*, 1996; *Sugi and Kawamura*, 1997; *Goswami*, 1998; *Ajayamohan and Goswami*, 2003; *Goswami and Xavier*, 2005; *Krishnan et al.*, 2009]. The ISMR also shows vigorous intraseasonal oscillations (ISOs), which manifest in active and break spells punctuating the seasonal evolution of the monsoon. Furthermore, ISOs and interannual variability (IAV) of ISMR are governed by a common mode of variability [*Goswami and Ajayamohan*, 2001]. Seasonal bias of the ISO anomalies contributes to the seasonal mean and it explains about half of the amplitude of the internal IAV [*Goswami and Xavier*, 2005]. Therefore, improved understanding of the mechanisms involved in the internal variability may enhance the predictability of ISMR.

Despite the importance of the internal variability on IAV, few studies attempted to understand its mechanism. *Krishnan et al.* [2009] have shown that monsoon rainfall variability may arise due to internal monsoon-midlatitude interactions. IAV may also arise due to modulation of the first positive phase of climatological ISO through internal land-atmosphere feedback [*Saha et al.*, 2011]. In many past studies, land-atmosphere interactions are recognized as one of the important sources of monsoon variability [*Shukla and Mintz*, 1982; *Webster*, 1983; *Meehl*, 1997; *Ferranti et al.*, 1999; *Koster et al.*, 2004;

Takata et al., 2009]. *Koster et al.* [2000] did a series of experiments with GCMs and found that amplification of precipitation variance by land-atmosphere feedback do take place in regions that are least affected by SST. *Ferranti et al.* [1999] have shown that the hydrological feedback enhances the low-frequency intraseasonal monsoon variability. *Webster* [1983]; *Srinivasan et al.* [1993] have suggested that moist processes of the land surface may have impact on the propagation of ISOs. However, recent study by *Jiang et al.* [2004] suggested that northward propagation of Indian summer monsoon ISO is essentially due to internal atmospheric dynamics and their theory is well accepted now. It is also observed that northward propagation of ISO becomes slower and rainfall intensity increases near the Indian land mass. Given the large scale nature of ISO, probably land surface processes have little effect on the genesis of ISO. However, regional interaction between ISO and land surface processes is possible and that may contribute in modifying the amplitude of ISO over the region north of 10 $^\circ$ N. As during active phase sky is mostly cloudy and the surface soil moisture remains at saturated level, stronger interaction between land and atmosphere through moisture and energy fluxes is expected only during break phase. We propose that soil moisture anomaly during a break phase causes anomalous changes in the atmospheric stability and this creates favorable/unfavorable conditions for the following active phase, which in turn modulates the intensity of rainfall over land and hence the seasonal rainfall.

The monsoon ISO arises from the convective coupling in the atmosphere [*Goswami and Shukla*, 1984; *Jiang et al.*, 2004; *Lau and Waliser*, 2005] and modified by the air-sea interactions. However, how it interacts with the prevailing land-surface conditions and to what extent it contributes to the intraseasonal rainfall variability are not well understood.

Anomalous soil moisture caused by active/break phase of ISO may persist for several days and this can cause the memory through anomalous moisture and energy fluxes. In general, a monsoon break (active) phase is characterized by scanty or no rainfall and clear sky (heavy rainfall and cloudy) condition over larger part of central India [*Ajayamohan and Goswami*, 2003]. Atmospheric instability may begin to grow from the initiation of a break condition through a combination of radiative cooling of the upper atmosphere and sensible heating of the lower atmosphere by the land surface. The lower atmospheric warming also depends on the available soil moisture and its partitioning into latent and sensible heat fluxes. Therefore, soil moisture anomaly during a break phase can alter the atmospheric stability, which in turn may influence the following active phase of ISO. Soil moisture anomaly during a break phase may arise due to scanty rainfall at that time only or through its memory of past event or both. Therefore, we hypothesize that there are inherent soil moisture and ISO feedback on the intraseasonal time scale and this can be one of the mechanisms through which seasonal bias of ISO anomaly is generated.

We show that such internal feedback is evident in the observed rainfall and multi-model analysis of land-surface data. Presence of such feedback is further demonstrated using two sets of internal simulation by a regional climate model (RCM). In order to test whether soil moisture anomaly during a break effects the following active phase, another sensitivity experiment by prescribing relatively wet (dry) soil moisture condition during break (active) is carried out. A detailed description of model setup and experimental design are given in section 2. Observed data sets used and methodology are described in section 3. Presence of inherent soil moisture and ISO feedback in the observed data is

discussed in section 4. Results from modeling experiment are presented in section 5 and conclusions are stated in section 6.

2. Model and Experiments

The regional climate model RegCM3 [*Pal et al.*, 2007] is used for this study. The dynamical core of RegCM is equivalent to the hydrostatic version of the fifth-generation Pennsylvania State University National Center for Atmospheric Research (NCAR), US, Meso-scale Model (MM5). The physical parametrization used in the simulations include the radiative transfer package of the NCAR Community Climate Model version 3 [CCM3, *Kiehl et al.*, 1996], the non-local boundary layer scheme by *Holtslag et al.* [1999] and mass flux cumulus cloud scheme of *Grell* [1993] with Fritsch and Chappell closure [*Fritsch and Chappell*, 1980]. Land-surface processes are described using the Biosphere-Atmosphere Transfer Scheme (BATS) [*Dickinson et al.*, 1993]. A standard model configuration with 18 vertical levels in the atmosphere (sigma coordinate) and $60km$ horizontal resolution with Normal Mercator map projection is used. The model domain covers the Indian subcontinent and its surrounding land and ocean part (40.2° - 116.3° E, 10.8° S - 47.7° N). In the lateral boundary and lower boundary, NCEP reanalysis [*Kalnay et al.*, 1996] six hourly data and Reynolds weekly sea surface temperature data [*Reynolds et al.*, 2002] respectively are used to force the model.

Though the lateral atmospheric boundary conditions and the lower boundary over ocean (SST) are prescribed, two-way regional interactions between land and atmosphere are present. These regional interactions also influence the large scale information, which is embedded on the boundary forcing and propagates into the model domain [e.g. *Denis et al.*, 2002; *Diaconescu et al.*, 2007]. Since the monsoon ISO also has larger spatial scale

[*Goswami and Ajayamohan*, 2001; *Goswami and Xavier*, 2005], modulation of it by internal land-atmosphere feedback is possible. In order to generate such internal variability, boundary conditions of a single year are used to force the model repeatedly year-after-year. Thus, two sets of internal simulation each of 31 years long, using boundary conditions of 1989 and 1983 are carried out. The control simulation shows that northward propagations during 1983 are very clear and strong [*Saha et al.*, 2011]. On the other hand, northward propagations in 1989 are rather weak. In reality, northward propagations of ISOs are not alike every year. In some year they are very strong and continuously propagate from the equator to about 30 ° N. However, in some year they are weak and discontinuous. Therefore, it is of interest to find out the internal land-atmosphere variability during these two types of years. The model is initialized with the boundary condition of 00 GMT 1^{st} January and for the successive run, restart file of preceding run is used. Hereafter the internal simulation will be referred as fixed boundary condition (FBC) experiment. Above boundary conditions happen to be of normal monsoon year. However, in principle, any boundary condition can be used for such experiment. IAV of the monsoon generated in the FBC experiments are clearly separated from all the slowly varying large scale influences (e.g. SST, snow cover etc) and attributed mainly to the regional land-atmosphere interactions.

Control simulations of 27 years (01-11-1981 to 31-12-2008) are carried out using lateral boundary forcing from NCEP and Reynold's SST at lower boundary. Model is initialized once at the beginning (00GMT 01-11-1981) and then integrated up to the end of December 2008. In order to find out whether soil moisture anomaly during a break effects the following active phase of ISO, another 27 years of sensitivity experiment by prescribing

smoothed annual cycle of soil moisture is carried out. Annual cycle of daily soil moisture (mean and first three harmonics) is constructed for all the grid points and all soil levels using daily soil moisture from the control simulation. The lateral and lower boundary conditions remained same as in the control run. Thus, year-to-year variability of soil moisture, which may be due to slowly varying large scale influences remained same, but the intraseasonal variability (which are internal) are removed. Furthermore, this experimental setup allows to have relatively wet (dry) soil condition in each and every break (active) phase (Figure S1). Similarly, another two sets of simulations each for eight years (01-11-1981 to 31-12-1989), but with a bigger domain (29.28° - 131.26° E, 30.64° S - 50.68° N) are carried out. Hereafter, control and sensitivity experiments with bigger domain are referred as Con-BD, Sen-BD respectively. This is to show whether feedback between soil moisture and ISO is sensitive to size of the model domain. Model experiments are summarized in Table 1.

3. Observed Data and Methods

India Meteorological Department (IMD) generated gridded (1°× 1°) daily rainfall data (1951-2007) [*Rajeevan et al.*, 2006] are used. There are very few measurements of soil moisture on regular basis over India [*Robock et al.*, 2000, 2003], which can show the existing relation between soil moisture and rainfall during the monsoon season. However, 1° gridded multimodel data from Global Soil Wetness Project-2 (GSWP-2) can be considered as land surface analog to the atmospheric reanalysis [*Dirmeyer et al.*, 2006]. Land surface models are forced with the best possible observation based 3-hourly estimates of near-surface meteorological fields [*Zhao and Dirmeyer*, 2003]. A comparison of rainfall data from GSWP-2 (which is also a model forcing field) with that of IMD reveals that, spatial

pattern of mean summer rainfall and the continuous wavelet spectra are quite similar to each other (Figure not shown). Though the feedback between land and atmosphere is excluded, use of best possible atmospheric forcing leads to more accuracy in the land-surface variables than what they lose in terms of consistency [*Liston et al.*, 1993; *Dirmeyer et al.*, 1999, 2006]. Therefore, the state of land-surface variables can be considered to be in equilibrium with the near-surface forcing fields and hence signature of feedback on longer time scale (i.e. on ISO time scale) may be seen through the relation between soil moisture and rainfall variability. Daily soil moisture and rainfall data of 10 years (1986-1995) are used for this study. For the analysis of atmospheric stability, 29 years (1979-2007) of daily pressure-level temperature and relative humidity from NCEP-II [*Kanamitsu et al.*, 2002] are used.

Central India (CI) (75.30°-86.63° E, 16.92°-26.43° N) represents a homogeneous summer monsoon rainfall region and hence the average rainfall over this region can be used for the monsoonal climate study [*Goswami et al.*, 2006]. Here, CI averaged time series from the model and observations is used for in-depth analysis. Daily anomalies are calculated by removing first three harmonics and mean from each year's time series.

4. Observed Land-Surface and ISO Interactions

4.1. In IMD Rainfall

Previous modeling studies have shown that intraseasonal variations of soil moisture do affect the rainfall by modulating amplitude and frequency of ISOs [e.g *Ferranti et al.*, 1999; *Webster*, 1983; *Srinivasan et al.*, 1993]. However, from observation it is difficult to find out whether anomalous surface-layer soil moisture can affect the monsoon rainfall significantly on intraseasonal time-scale. If the feedback contributes significantly towards

the modulation of ISO, that evidence may be seen in the intraseasonal variation of rainfall itself. As there is little or no rain during a break phase, it may be considered a relatively dry period. Therefore, anomalous rainfall during a break phase (which may not be of large spatial scale and intensity) can introduce large variability in the soil moisture and hence in the stability of the atmospheric boundary layer (ABL), i.e. an increase (decrease) in soil moisture can decrease (increase) the ABL temperature and that may induce more (less) stability in the atmosphere. Furthermore, anomalous rainfall can also induce stability by itself, through increase in temperature at the upper level (through release of latent heat). As a consequence, more (less) stability during a break phase may not be the favorable (unfavorable) condition for the following active phase. Thus, it is expected that a weaker break phase (relatively wet) is followed by weaker active phase and a stronger break is followed by stronger active phase.

In order to examine this relation, monsoon ISO index (MII) is constructed by using CI averaged 10-90 days filtered rainfall anomaly (JJAS) and then normalized by its own standard deviation. The MII index is normally distributed and the standard deviation of filtered rainfall anomaly is $2.3\,mm$ (figure not shown). Therefore, MII= 2 represents rainfall anomaly of $\pm 4.6\,mm$, which is also about 2^{nd} and 97^{th} percentile of the whole time series. Therefore, if MII $\geq$ 2 (1 $\geq$ MII $<$ 2), it is considered as a strong (weak) active phase. Thus, in total 49 strong and 156 weak active phases are identified using 57 years of IMD rainfall data (1951-2007). Figure 1b shows the composite of strong and weak active rainfall with 25 days lead/lag time. Weak (strong) active phases are indeed preceded and followed by significantly more (less) amount of rainfall (above 90% significance level). The composite of 10-90 days filtered rainfall anomaly also shows similar features as in the

total rainfall. However, from here time length of the lagged response of rainfall to the soil moisture anomaly is not clear. It is expected to be about half of the period of ISO (i.e. about 10-20 days, Figure 1b), but state of atmospheric conditions during a break phase may also be influenced by the soil moisture memory of previous active phase rainfall. As a result, the time lag is expected to be more than simply half of the ISO period.

To further support our hypothesis, vertical gradient of equivalent potential temperature (GEPT), based on CI averaged temperature and humidity from NCEP-II reanalysis [*Kanamitsu et al.*, 2002] is calculated. For the lead/lag composite, dates are taken from MII based on IMD rainfall. Negative slope of GEPT during lead/lag period suggests unstable condition in the lower atmosphere (Figure 1c). It may be noted that low-level atmosphere (below 600 hPa) is more unstable during lag time than that of lead time, which further suggest that a strong unstable condition prior to the peak of rainfall is followed by relatively stable condition. Difference between strong and weak composite of GEPT depicts that during the lag (lead) time, low-level atmosphere is more unstable (stable) for strong active phase as compared to the weak active phase. Therefore, a strong active phase is preceded (followed) by more (less) unstable conditions and thus reduces the convective activity of the following active phase. These feedback are shown by schematic diagram in Figure 2. NCEP-I reanalysis also shows similar result, but the vertical gradient is slightly weaker as compared to the NCEP-II (Figure not shown). A strong active phase can pour more moisture into the soil as compared to a weak active phase, which in turn causes strong memory in the soil. This creates more stabilization at the low-level atmosphere during the following break phase. Therefore, a heavy rain from strong active phase can amplify the following break.

4.2. In GSWP-2

Wavelet spectra of CI averaged surface soil moisture (top 10 cm average) and rainfall anomaly for JJAS show significant power at 10-20 and 30-60 days band (Figures 3a, 3b). Amplitude as well as the number of active/break phases of ISO vary from year to year. Though the intraseasonal and interannual variability have common mode of spatial structure [*Goswami and Ajayamohan*, 2001; *Fujinami et al.*, 2011], all of the ISOs are not clearly separated from high frequency synoptic events and hence only some of them are statistically significant. On the other hand, variation of soil moisture takes place on a longer time scale and hence possesses a longer memory. Therefore, wavelet spectra of soil moisture show significant power, which persist for longer period as compared to rainfall.

The cross wavelet transform of the soil moisture and rainfall shows features which are common to both time series (Figures 3c), i.e. both have high power at 10-20 and 30-60 days band and that is present almost in each year. Common significant power with longer duration at 30-60 days band further reveals the feedback nature of land and atmosphere, where the former varies slowly. Vectors indicate phase difference between soil moisture and rainfall anomaly (with in-phase pointing right, anti-phase pointing left and vertically upward indicates rainfall lags the soil moisture by 90 °). It may be noted that within the time span of 10 years, relation between the soil moisture and the rainfall is statistically stationary and most of the time either they are in phase or the rainfall lags the soil moisture. Therefore, part of the ISO variability may be linked with the internal land-atmosphere feedback.

Autocorrelation of surface soil moisture decreases rapidly below significance level by about 7-12 days and then reaches to minimum by about 17-40 days (Figure 4). In some

year, correlation minima again start to increase and reach positive maxima by about 27-60 days, which also imply dominant period of variation in the soil moisture. Similar variations are also evident in the deeper soil layer, but with longer time lag (figure not shown). Here, we have used daily soil moisture of the months May to September (i.e. 151 days). Though, the climatological onset date at southern peninsular India is 1^{st} June and it takes about two weeks to cross central India, there are many years when onset was in the month of May. Furthermore, the result does not change much even if we use JJAS daily data. Surface layer is exposed to the fast varying atmospheric processes, which control the surface soil moisture variability. On the other hand, soil moisture at the deeper layer is governed by relatively slow processes like sub-surface drainage and infiltration. During dry atmospheric conditions, upward transport of moisture from the deeper layer also induces inertia into the surface layers and hence increases the memory. This helps to maintain a colder boundary layer through increased surface evaporation and evapotranspiration by vegetation. Therefore, a positive soil moisture anomaly may induce negative rainfall anomaly within the period of about 2-6 weeks, or in other words, a strong break phase may lead to a strong active phase and vice versa, provided both phases occur within the limit of soil moisture memory. Existence of such soil moisture variability is further demonstrated by two sets of FBC experiment (section 5.2).

5. Results from Model Simulation

5.1. Monsoon in Control Simulation

RegCM3 is able to simulate the basic features of the monsoonal climate [*Ratnam et al.*, 2009; *Ashfaq et al.*, 2009]. A similar model setup as described in section 2 is used for 27 years of long simulation over the same domain by *Saha et al.* [2011]. The model

overestimates seasonal summer monsoon rainfall over Arabian Sea and Bay of Bengal, but it is able to capture the rainfall pattern over land quite well. The location of low-level and upper level monsoon Jets, their magnitude and northward propagation of ISOs are simulated reasonably well in the model (see *Saha et al.* [2011] for details).

5.2. Internal Feedback in FBC Experiment

There are four (three) active phases in the FBC-1989 (FBC-1983) experiment, which are evident from 20-100 days filtered CI averaged rainfall anomaly (Figures 5a,6a). Positive (negative) regions are representative of active (break) phase of the monsoon ISO. It may be noted that phase of ISOs did not change much from year-to-year, but there are large variations in the amplitude. *Diaconescu et al.* [2007] have shown that large scale signal present in the lateral boundary forcing, propagates into the model domain and retains its large scale features. As ISOs are also large scale phenomena and the boundary conditions remain same, the timing of the active, break events is expected to be same for all the years and that is what exactly seen in Figures 5a,6a. Though, the year-to-year variation of ISO amplitude has no physical link, but within a season variation may be generated due to internal land-atmosphere feedback. Within a year, below (above) normal negative (positive) rainfall anomaly is followed by above (below) normal positive (negative) rainfall anomaly. Initiation of the first anomaly is very likely from the non linearity in the system. However, once there is an anomaly, it follows a deterministic path. These variations also corroborate the observed features of strong and weak ISO composite from IMD rainfall (Figure 1) and autocorrelation of soil moisture from GSWP-2 (Figure 4). Use of 10-100 days filtered anomaly also depicts similar features, but as the power in 30-60 days band is much higher, variations are more clearly seen in 20-100 days filtered anomaly.

CI averaged seasonal mean and interannual standard deviation of rainfall in the FBC-1989 (FBC-1983) are 83.82 cm and 2.59 cm (88.55 cm and 2.49 cm) respectively (Figures 5b,6b). Mean and standard deviation in the 27 years of control simulation are 86.54 cm and 7.08 cm respectively. Therefore, about 35% of interannual rainfall variation is generated internally. However, from here it is not clear whether the IAV is through the modulation of ISO. Seasonal average of ISO anomalies can be positive or negative and its amplitude may vary from year to year depending on the number as well as amplitude and duration of the active/break events. Since the number of active and break events are fixed, the only possibility is through the modulation of ISO amplitude. The scatter diagram of ISO bias and seasonal rainfall anomaly shows that they are strongly related (Figures 7a, 7b) and about 20-30% of interannual rainfall variation is due to ISO bias. Therefore, it is evident from the FBC experiments that amplitude of ISOs can be modulated by the internal feedback, presumably by the land-atmosphere interactions and those can generate IAV. It appears that anomalous soil moisture during a break phase triggers anomalous changes in the following active phase and afterward this anomaly has effect on the following break phase. This is further demonstrated through a sensitivity experiment in section 5.3.

Now using autocorrelation we show the time scale and robustness of this feedback. Since in the FBC experiment, boundary conditions remain same for each year, the phase locked component of ISOs (i.e. climatological ISO) is quite strong and does not change much from year-to-year. However, deviations of ISOs from their climatological mean are due to the internal dynamics. Therefore, surface (top 10 cm layer) soil moisture anomalies for each 31 years are constructed by removing daily climatology mean from the time series (May to September). Autocorrelations drop below significance level by 3-28 (3-14) days lag

in the FBC-1989 (FBC-1983) experiment and afterward become significantly negative for wide range of lagged days (Figure 8a, 8b). Lag day, where positive correlation drops below significance level indicates the persistence of influence to reoccur the event with same sign. On the other hand, lag day where negative correlation becomes significant indicates the persistence of influence to reoccur the event with opposite sign. Furthermore, lag days in many years (both positive and negative correlations significant above 95% level) are within monsoon intraseasonal time scale. It may be noted that autocorrelations for FBC-1989 experiment are much stronger than that of FBC-1983. Above differences may be linked with the strength of ISO phases. A strong active (break) phase of ISO may refill (dry out) the soil moisture to such an extent that memory of previous events are almost lost. Since the data length used for each year is not very long (153 days; May-September), correlation beyond 40-50 days lag may not be very reliable. Despite that, evidence of interactions of an ISO anomaly with the following ISO event is statistically robust. One possibility to test whether soil moisture memory affects the ISO (i.e. weak break followed by weak active phase) is by removing intraseasonal variability and prescribing in a similar set of simulation as in the control.

5.3. Prescribed Soil Moisture Experiment

In the prescribed soil moisture experiment, not only the intraseasonal variation of soil moisture is removed, but also it provides relatively wet condition before an active ISO phase (Figure S1). Therefore, it is expected that atmospheric stability will increase before an active phase (i.e. during a break condition) as compared to the control simulation. Exactly same boundary conditions as in the control simulation also ensure that phase of ISOs do not change much (Figure S2). Average shift in the peak of an active (a break)

date in the sensitivity experiment as compared to the control simulation is about 8-9 (10-14) days. This experiment further ensures the reproducibility of ISOs with quite similar phase. Thus, if there is any influence of break phase soil moisture on the following active phase, it will affect the seasonal mean monsoon through the modulation of ISOs.

5.3.1. Effects on Mean Monsoon

CI averaged seasonal mean (JJAS) rainfall is decreased in the sensitivity experiment by $0.9\,cm$ and the interannual standard deviation of seasonal rainfall is increased by $0.62\,cm$ (Figure S3a). The year-to-year difference between control and sensitivity is remarkable, where the interannual standard deviation is 3.41cm (Figure S3b). Difference of CI averaged seasonal rainfall is normalized by its own standard deviation. It may be noted that in most of the years when difference is large (± 1 s.d.), the seasonal rainfall is suppressed in the sensitivity experiment. The spatial pattern of seasonal rainfall captured by the model in both runs is quite similar to each other, but the mean rainfall is decreased in the sensitivity experiment over CI, adjoining Arabian Sea and Bay of Bengal by maximum of $3\,cm$ (Figure not shown).

Monsoon is characterized by divergence in the upper troposphere with a maximum in the vertical motion at about 400 hPa and convergence in the lower troposphere with a maximum at 925/850 hPa [*Trenberth et al.*, 2000], where the low-level convergence is balanced by the upper-level divergent flow. In the control and sensitivity experiment, locations of the low-level (850 hPa) monsoon Jet over Arabian sea, cross equatorial flow and easterly winds at the south of the equator are very similar to each other (Figures 9a, 9b). Tibetan anticyclone around 30° N and easterly Jet around 5° N are also well captured by the model (Figures 9d, 9e). However, wind speed in the model is slightly

stronger as compared to NCEP reanalysis (see *Saha et al.* [2011] for details). The difference between control and sensitivity resembles to the pattern, which is very similar to the observed anomalous wind during an active phase [see *Goswami and Ajayamohan*, 2001]. Therefore, weaker low-level monsoon Jet over Arabian Sea along with weaker upper level easterly over the same region indicate weakening of the mean monsoon circulation in the sensitivity experiment.

According to Helmholtz's theorem, wind can be separated into rotational and divergent component [e.g. *Behera et al.*, 1999]. Divergent component of moisture flux (vertically integrated $q\vec{V}$ from surface to 300 hPa) during JJAS shows the center of moisture convergence at about 90° E, 30° N (Figure 11). The positive (negative) velocity potential (shaded region in Figure 11a) represents the region of convergence (divergence). Similar divergent and convergent patterns are also seen in NCEP reanalysis data (not shown). The sensitivity experiment clearly indicates decrease in the moisture convergence over Indian sub-continent (Figure 11b). Overall the convergence/divergence is weaker in the sensitivity experiment as compared to the control simulation. Above differences are also consistent with the weakening of the mean monsoon circulation.

5.3.2. Modulation of ISOs

ISO variance of JJAS rainfall (10-90 days filtered anomaly) from control and sensitivity experiment is shown in Figure 10a,10b respectively. The model has large bias in the mean rainfall over Arabian Sea and Bay of Bengal [*Saha et al.*, 2011] and the rainfall variance is also biased by and large over the same regions. However, rainfall variance in the sensitivity experiment is decreased significantly over CI (significant at 99% level, Figure 10c). The area of maximum ISO bias shows minimum difference. Similarly, ISO

variance of wind speed at 850 hPa shows maxima at the region between 10-20° N and at around south of the Equator and 78° E (Figure 10d,10e). Above regions also coincide with the Jets in mean wind at 850 hPa. A decrease in variance (significant at 99% level) of low-level wind over western Arabian Sea is evident in the sensitivity experiment (Figure 10f), which again implies the weakening of ISO due to the absence of intraseasonal soil moisture variability. However, from here it is not clear whether both phases of the ISO (active and break) have become weaker.

In order to investigate the changes during active/break phase, composites of strong ISOs during active (MII$\geq$ 1) and break phases (MII≤ -1) are constructed. Strong ISOs are identified in a similar way as in the case of IMD rainfall (i.e |MII| $\geq$ 2). Primary supply of moisture for the monsoon rainfall is through advection from ocean. However, local evaporation, i.e. recycling of moisture also contributes to the total rainfall (about 10-15% over CI in the model). Therefore, P-E (Precipitation - Evaporation) may be the appropriate quantity to look at for the changes, which is caused by large-scale moisture advection. The active phase is characterized by intense large-scale rainfall over CI, foothills of Himalaya and western coast (Figure 12a). Contrary to that, break phase is characterized by very little or no rainfall over a wide region of CI and decreased intensity over western coast region (Figure 12c). Difference between control and sensitivity of above composites is shown in Figures 12b, 12d. It turns out that P-E during active phase is decreased significantly in the sensitivity experiment over western ghat and CI. On the other hand during break phase, there is moderate decrease in P-E over part of CI and increase beside the area where mean rainfall is quite high and that may be linked with the advection of moisture from increased evaporation (Figure 12h). Mean spatial pattern of evaporation

during active and break phases is very similar to the rainfall pattern (Figure 12e,g). Since the soil moisture is prescribed in the sensitivity experiment, atmospheric conditions are the only limiting factors for evaporation. As a result, prescribed soil moisture acts as infinite source and increases local evaporation in the sensitivity experiment. Therefore, net rainfall increases during break period over CI, north and north-west India (Figure not shown).

Decrease in P-E during active phase is further supported by weaker monsoon circulation at 850 hPa (Figure 13a). Cross equatorial flows including Somali Jet are significantly weaker in the sensitivity experiment. On the other hand, 850 hPa wind during break phase also becomes weaker, but changes are confined to north of the equator and on a relatively smaller scale (Figure 13b). Since soil moisture is prescribed, it acts as an infinite source and evaporates whenever atmospheric conditions become favorable for the evaporation (mainly during break). As a result, surface temperature also becomes colder and hence land-ocean temperature gradient decreases (Figure not shown). This may explain why the wind circulation during break phase also becomes weaker, despite increase in rainfall. Southerly wind over CI and north of 20° N are increased, which is consistent with increased rainfall during break phase. We recall that the sensitivity experiment is designed to have wetter condition during break phases and that is exactly found here.

Now we examine whether changes in the rainfall are linked with the large-scale moisture convergence. Divergent component of moisture flux (vertically integrated $q\vec{V}$ from surface to 300 hPa) during active phase shows the center of moisture convergence at about 85° E, 26° N (Figure 14a). However, during break phase the center of moisture convergence is shifted towards east (95° E, 26° N; Figure 14c). There is significant decrease in mois-

ture convergence in the sensitivity experiment over a wide region of Indian sub-continent (Figure 14b). On the other hand, during break phase the divergence over southern India and northern Indian ocean (centered around 5° N, 75° E) is weaker (Figure 14d). This further implies that increased rainfall during break is not caused by the changes in the large-scale features of monsoon. Contrary to that, interaction of soil moisture anomaly with atmosphere triggers changes in the large scale moisture convergence during active phase and hence modulates the ISO. As the active and break phases are identified based on the rainfall over CI and there is phase shift between control and sensitivity experiment, significant area beyond the monsoon region ($\approx$ north of 35° N) may not have physical reasoning. They may be caused simply by phase shift in the composite, which is part of the large-scale information (driven by the boundary conditions) and does not differ much between control and sensitivity experiment.

Similar to OLR, moist static energy (MSE) also indicates the region with high convective activity and can be used as a measure of instability [e.g. *Srinivasan and Smith*, 1996]. Larger values of surface level MSE (average from surface to 700 hPa) spread over Asian monsoon region during both active and break phase clearly indicate the region of high instability (Figure 15a, 15c). MSE with maximum value during active phase is centered over Indian subcontinent and it moves towards the east during break phase. Since the prescribed soil moisture in the sensitivity experiment regulates the low-level temperature and humidity, MSE is also changed throughout the domain. However, equal change in MSE over high latitude with lower mean value as compared to the monsoon region may not be important in terms of changes in the convective instability. Therefore, changes in the MSE during active and break phase over the region with mean $\geq 335\,kJ\,kg^{-1}$, which

covers the monsoon region (Figure 15b, 15d) are presented. Interestingly, MSE during both phases becomes weaker and hence supports the hypothesis of internal soil moisture and ISO feedback.

Stability of the lower atmosphere can also be inferred from the vertical gradient of equivalent potential temperature ($\frac{d\theta_e}{dz}$), which is controlled by both, temperature and available moisture in the atmosphere. As the boundary layer warms up during break phase, the lower atmosphere becomes more unstable than the active phase, which is evident from Figure 16a,b. Further analysis shows a decrease of 1.2 $^\circ$ C (0.2 $^\circ$ C) in low-level atmospheric temperature (CI averaged and from surface to 850hPa) during break (active) phase. While, change in the vertical profile of humidity (CI averaged) during break is not so significant, a strong and systematic decrease in humidity (from surface to 300 hPa) is found during active phase (figure not shown). These together result into increased instability at the near surface (surface to 850 hPa) and decreased instability within 850 hPa to about 500 hPa level (Figure 16c). Therefore, as we hypothesized, wet soil moisture anomaly during break produces more stability and that reduces the large scale convection in the following active phase.

Power spectra of CI averaged daily JJAS rainfall anomaly show the ability of the model to capture 10-20 and 30-60 days modes of ISO (Figure 17). The spectral bands of ISOs in the sensitivity experiment are very similar to the control and the variances are reduced mainly on those of ISO bands (marked by thick ellipse) except at about 25 days period, where it is increased. As a result, seasonal mean monsoon and therefore, seasonal rainfall in the sensitivity experiment is not always less than the control simulation. This discrepancy may be the result of non-linear interactions between ISO bands and high frequency

synoptic events [*Goswami and Xavier*, 2005]. Therefore, power spectra further confirm that decreased atmospheric stability caused by positive anomaly of soil moisture during a break phase does affect the amplitude of active phase rainfall.

5.4. Sensitivity to Model Domain Size

In principle, soil moisture and ISO feedback can be seen clearly in the simulation with bigger domain, provided there is no other major internal feedback outside the monsoon region which influences the former through teleconnections. Similar to the control and sensitivity experiment, active and break composites are also calculated using data from eight years of Con-BD and Sen-BD experiments. P-E during strong active shows large scale pattern over CI, which is quite similar to the simulation with smaller domain (Figure S4). It may be noted that decrease in P-E in the Sen-BD experiment is much larger during strong active phase and over the maximum rainfall region. On the other hand, there is marginal increase/decrease in P-E during strong break phase. Also, evaporation is increased during break in the Sen-BD over central and north-west part of India. Weakening of low-level monsoon circulation in Sen-BD as compared to Con-BD during both active and break is also evident (Figure S6). Decrease in the vertically integrated moisture convergence further shows that active phage of monsoon becomes weaker because of wet soil condition during previous break phase. All these match quite well with the experiment using smaller domain (i.e. section 5.3). Therefore, the statistics of regional feedback between ISOs and soil moisture is not dependent on the domain size. This implies that physics of regional land-atmosphere interactions does not change with the size of the model domain.

6. Summary

Land surface is believed to be one of the most important components, which can introduce variability into the monsoon system. However, mechanism through which it interacts with the monsoon, particularly the ISO is not well established. Here, we have presented a mechanism through which amplitude of ISOs can be modulated by internal intraseasonal land-atmosphere feedback. It is proposed that soil moisture anomaly during a break (active) phase causes anomalous changes in the atmospheric stability and this creates favorable/unfavorable condition for the following active (break) phase, which in turn modulates the intensity of rainfall over land and contributes to the seasonal anomaly.

Composite of the observed rainfall ISOs indicates that there is inherent land-atmosphere feedback, which influences the amplitude of rainfall during an active phase in the following sequence: An increase (decrease) in rainfall during a break phase is followed by a weaker (stronger) active phase and then followed by a weaker (stronger) break phase. Autocorrelation of soil moisture from GSWP-2 further indicates the persistence of influence to reoccur the event with opposite sign on time scale of the monsoon ISO and thus supports the hypothesis.

Similar feedback, as evident in the IMD rainfall and GSWP-2 soil moisture data is demonstrated using two sets of internal simulation (i.e. FBC experiments) by a regional climate model. A strong correlation between seasonal mean of ISO anomaly and seasonal anomaly in the FBC experiment further confirms the role of internal land-atmosphere feedback on modulation of the amplitude of ISOs and hence, the IAV of monsoon rainfall. It is also found that about 20-30% seasonal rainfall anomaly is due to seasonal average of ISO anomaly and the remaining part may be due to high frequency variability or sim-

ply the noise. In order to confirm whether soil moisture anomaly during a break phase has effect on the following active phase, a sensitivity experiment by prescribing smoothed annual cycle of soil moisture from control simulation is carried out. Hence, in the sensitivity experiment, wet (dry) soil moisture condition prevailed during all the break (active) phases. It turns out that the seasonal rainfall decreases in the sensitivity experiment during most of the years. However, for very few years it is just opposite. As proposed, amplitude of rainfall and wind ISOs becomes weaker in the sensitivity experiment. Increase in rainfall during a break phase is linked mainly with the local processes and that results into more stability in the atmospheric. However, decrease in rainfall during an active phase is associated with decrease in the large scale monsoon circulation, moisture convergence and increase in the atmospheric stability over CI.

As the model is constrained by one-way interactions at the lateral boundary and ISOs are on very large scale, the size of model domain may limit the results. In order to reconfirm the findings, control and sensitivity experiments using a much larger domain are carried out. It turns out that the nature of soil moisture and ISO feedback over Indian subcontinent is not sensitive to the domain size, which is larger by 50%. Therefore, as hypothesized, positive soil moisture anomaly during a break phase increases the atmospheric stability and that leads to a weaker monsoon circulation in the following active phase.

The interaction involved in the model is one-way, i.e. large scale atmospheric conditions interact with the land-surface processes in the monsoon region, but how they perturb the large scale monsoon system is not clear from this study. However, it is able to separate internal and external (i.e. slowly varying large scale) processes. As a result, importance

of land-surface condition on the monsoon ISO variability is clearly brought out. Soil moisture and ISO feedback may have important implication in terms of improved initial soil moisture condition in dynamical prediction model, which may in turn improve the monsoon rainfall forecast.

Acknowledgments. We thank Abdus Salam International Centre for Theoretical Physics in Trieste, Italy for making available the model codes of RegCM3 for this study. We thank three anonymous reviewers for their constructive suggestions, which improved the manuscript. Fellowship of Subhadeep Halder is funded by CSIR, New Delhi.

References

Ajayamohan, R. S., and B. N. Goswami, Potential predictability of the asian summer monsoon on monthly and seasonal time scales, *Meteor. Atmos. Phys.*, pp. doi:10.1007/s00,703–002–0576–4, 2003.

Ashfaq, M., Y. Shi, W. w. Tung, R. J. Trapp, X. Gao, J. S. Pal, and N. S. Diffenbaugh, Suppression of south asian summer monsoon precipitation in the 21^{st} century, *Geophys. Res. Lett.*, *36*, doi:10.1029/2008GL036,500, 2009.

Behera, S. K., R. Krishnan, and T. Yamagata, Unusual ocean atmosphere conditions in the tropical indian ocean during 1994, *Geophys. Res. Lett.*, *26*, 3001 – 3004, 1999.

Denis, B., R. Laprise, D. Caya, and J. Côté, Downscaling ability of one-way nested regional climate models: the big-brother experiment, *Clim. Dyn.*, *18*, 627 – 646, 2002.

Diaconescu, E. P., R. Laprise, and L. Sushama, The impact of lateral boundary data errors on the simulated climate of a nested regional climate model, *Clim. Dyn.*, *28*, 333–350, 2007.

Dickinson, R. E., A. Henderson-Sellers, and P. J. Kennedy, Biosphere-atmosphere transfer scheme (bats) version 1e as coupled to the ncar community climate model, *NCAR Technical Note NCAR/TN-387+STR*, National Center for Atmospheric Research, Boulder, CO, 1993.

Dirmeyer, P. A., A. J. Dolman, and N. Sato, The pilot phase of the global soil wetness project, *Bul. Amer. Meteor. Soc.*, *80*, 851–878, 1999.

Dirmeyer, P. A., X. Gao, M. Zhao, Z. Guo, T. Oki, and N. Hanasaki, Gswp-2 - multimodel analysis and implications for our perception of the land surface, *Bul. Amer. Meteor. Soc.*, *87*, 1381–1397, 2006.

Ferranti, L., J. M. Slingo, T. N. Palmer, and B. J. Hoskins, The effect of land-surface feedbacks on the monsoon circulation, *Q. J. R. Meteorol. Soc.*, *125*, 1527–1550, 1999.

Fritsch, J. M., and C. F. Chappell, Numerical prediction of convectively driven mesoscale pressure systems. part i: Convective parameterization, *J. Atmos. Sci.*, *37*, 1722 – 1733, 1980.

Fujinami, H., et al., Characteristic intraseasonal oscillation of rainfall and its effect on interannual variability over bangladesh during boreal summer, *Int. J. Climatol.*, *31*, 1192 – 1204, 2011.

Goswami, B. N., Interannual variations of indian summer monsoon in a gcm: External conditions versus internal feedbacks, *J. Clim.*, *11*, 501 – 522, 1998.

Goswami, B. N., and R. S. Ajayamohan, Intraseasonal oscillation and interannual variability of the indian summer monsoon, *J. Clim.*, *14*, 1180 – 1198, 2001.

Goswami, B. N., and J. Shukla, Quasi-periodic oscillation in a symmetric general circulation model, *J. Atmos. Sci.*, *41*, 20 – 37, 1984.

Goswami, B. N., and P. K. Xavier, Dynamics of internal interannual variability of the indian summer monsoon in a gcm, *J. Geophys. Res.*, *110*, D24,104, doi:10.1029/2005JD006,042, 2005.

Goswami, B. N., V. Venugopal, D. Sengupta, M. S. Madhusoodanan, and P. K. Xavier, Increasing trend of extreme rain events over india in a warming environment, *Science*, *314*, 1442 – 1445, 2006.

Grell, G. A., Prognostic evaluation of assumptions used by cumulus parameterization, *Mon. Weather Rev.*, *121*, 764 – 787, 1993.

Holtslag, A. A. M., E. I. F. D. Bruijn, and H. L. Pan, A high resolution air mass transformation model for short-range weather forecasting, *Mon. Weather Rev.*, *118*, 1561 – 1575, 1999.

Jiang, X., T. Li, and B. Wang, Structures and mechanisms of the northward propagating boreal summer intraseasonal oscillation, *J. Clim.*, *17*, 1022 – 1039, 2004.

Kalnay, E., et al., The ncep/ncar 40-year reanalysis project, *Bul. Amer. Meteor. Soc.*, *77*, 437–470, 1996.

Kanamitsu, M., W. Ebisuzaki, J. Woollen, S.-K. Yang, J. J. Hnilo, M. Fiorino, and G. L. Potter, Ncep-deo amip-ii reanalysis (r-2), *Bul. Amer. Meteor. Soc.*, *83*, 1631 – 1643, 2002.

Kiehl, J. T., J. J. Hack, G. B. Bonan, B. A. Boville, B. P. Briegleb, D. L. Williamson, and P. J. Rasch, Description of the ncar community climate model (ccm3), *Tech. rep.*, NCAR, NCAR/TN-420+STR,, 1996.

Koster, R. D., M. J. Suarez, and M. Heiser, Variance and predictability of precipitation at seasonal-to-interannual timescales, *J. Hydro. Meteorol.*, *1*, 26–46, 2000.

Koster, R. D., et al., Regions of strong coupling between soil moisture and precipitation, *Science*, *305*, 1138–1140, 2004.

Krishnan, R., V. Kumar, M. Sugi, and J. Yoshimura, Internal-feedbacks from monsoon-midlatitude interactions during droughts in the indian summer monsoon, *J. Atmos. Sci.*, *66*, 553–578, 2009.

Lau, W. K.-M., and D. E. Waliser, *Intraseasonal Variability in the Atmosphere-Ocean Climate System*, Springer Praxis Publishing Ltd., section 2: South Asian Monsoon, by B. N. Goswami, 2005.

Liston, G. E., Y. C. Sud, and G. K. Walker, Design of a global soil moisture initialization procedure for the simple biosphere model., *NASA Tech. Memo. 104590*, Goddard Space Flight Center, Greenbelt, MD, 1993.

Meehl, G. A., The south asian monsoon and the tropospheric biennial oscillation, *J. Clim.*, *10*, 1921 – 1943, 1997.

Pal, J. S., et al., Regional climate modeling for the developing world: The ictp regcm3 and regcnet, *Bul. Amer. Meteor. Soc.*, *88 (9)*, 1395–1409, 2007.

Rajeevan, M., J. Bhate, J. D. Kale, and B. Lal, High resolution daily gridded rainfall data for indian region: Analysis of break and active monsoon spells, *Curr. Sci.*, *9(3)*, 296 – 306, 2006.

Ratnam, J. V., F. Giorgi, A. Kaginalkar, and S. Cozzini, Simulation of the indian monsoon using the regcm3roms regional coupled model, *Clim. Dyn.*, *33*, 119–139, 2009.

Reynolds, R. W., N. A. Rayner, T. M. Smith, D. C. Stokes, and W. Wang, An improved in situ and satellite sst analysis for climate, *J. Clim.*, *15*, 1609 – 1625, 2002.

Robock, A., K. Y. Vinnikov, G. Srinivasan, J. K. Entin, S. E. Hollinger, N. A. Speranskaya, S. Liu, and A. Namkhai, The global soil moisture data bank, *Bul. Amer. Meteor. Soc.*, *81*, 1281–1299, 2000.

Robock, A., M. Mu, K. Vinnikov, and D. Robinson, Land surface conditions over eurasia and indian summer monsoon rainfall, *J. Geophys. Res.*, *108*, 4131–4143, 2003.

Saha, S. K., S. Halder, K. K. Kumar, and B. N. Goswami, Pre-onset land surface processes and 'internal' interannual variabilities of the indian summer monsoon, *Clim. Dyn.*, *36*, 2077–2089, 2011.

Shukla, J., and Y. Mintz, Influence of land-surface evapotranspiration on the earth's climate, *Science*, *215*, 1498–1501, 1982.

Sperber, K. R., and T. N. Palmer, Interannual tropical rainfall variability in general circulation model simulations associated with the atmospheric model intercomparison project, *J. Clim.*, *9*, 2727 – 2750, 1996.

Srinivasan, J., and G. L. Smith, The role of heat fluxes and moist static energy in tropical convergence zones, *Mon. Weather Rev.*, *124*, 2089–2099, 1996.

Srinivasan, J., S. Gadgil, and P. J. Webster, Meridional propagation of large-scale monsoon convective zones, *Meteor. Atmos. Phys.*, *52(1-2)*, 15–35, doi: 10.1007/BF01025,750, 1993.

Sugi, M., and R. Kawamura, A study of sst-forced variability and potential predictability of seasonal mean fields using the jma global model, *J. Meteor. Soc. Jap.*, *75*, 717 – 736, 1997.

Takata, K., K. Saito, and T. Yasunari, Changes in the asian monsoon climate during 1700-1850 induced by preindustrial cultivation, *Proc. Natl. Acad. Sci. USA*, *106*, 9586

– 9589, 2009.

Trenberth, K. E., D. P. Stepaniak, and J. M. Caron, The global monsoon as seen through the divergent atmospheric circulation, *J. Clim.*, *13*, 3969 – 3993, 2000.

Webster, P. J., Mechanisms of monsoon low-frequency variability: Surface hydrological effects, *J. Atmos. Sci.*, *40*, 2110–2124, 1983.

Zhao, M., and P. A. Dirmeyer, Production and analysis of gswp-2 near-surface meteorology data sets, *COLA Technical Report 159*, Center for Ocean-Land-Atmosphere Studies, 4041 Powder Mill Road, Suite 302, Calverton, MD 20705 USA, 2003.

Figure 1. CI averaged lead/lag composite of ISO phases. Strong (red line) and weak (blue line) active composite of a) 10-90 days filtered rainfall anomaly and b) total rainfall using 1951-2007 IMD data. Shaded area are significant at 90% level. c) Strong active composite of the vertical gradient of equivalent potential temperature ($\frac{d\theta_e}{dz}$ in °C km^{-1}; black contour) and strong active minus weak active composite of $\frac{d\theta_e}{dz}$ (shaded color) using 1979-2007 NCEP-II reanalysis data. Green contours show significance at 90% level.

Figure 2. Schematic diagram of feedback loop. Thick arrows with solid (dashed) out line represents the positive (negative) feedback.

Figure 3. Continuous wavelet power spectrum of CI averaged daily(JJAS) a) soil moisture (top 10 cm) and b) rainfall from GSWP-2 (shaded color is continuous wavelet power, normalized by variance of the time series). c) Cross wavelet transform of above rainfall and soil moisture time series (shaded color is cross wavelet power of standardized time series and vectors represent the phase angle). Black thick contours represent the 95% significance level and the cone of influence where edge effects might distort the picture is shown as a lighter shade.

Figure 4. Autocorrelation of CI averaged daily (May to September) soil moisture anomaly (10cm) from GSWP-2. Thick red lines indicates the 95% significance level. Thin black curves represent autocorrelation of each individual year (1986-1995).

Figure 5. From the FBC-1989 experiment, a) CI averaged 20-100 days filtered rainfall anomaly ($mm\,day^{-1}$) for all 31 years. Black arrows indicates the link between anomalous break and active phases within a year. b) CI averaged seasonal rainfall anomaly, normalized with its own standard deviation.

Figure 6. Same as Figure 5 but for FBC-1983 experiment.

Figure 7. Scatter plot of CI averaged seasonal rainfall anomaly (in mm) versus seasonal average of 10-90 days filtered rainfall anomaly (in mm) from a) FBC-1989 and b) FBC-1983 experiment.

Figure 8. Autocorrelation of CI averaged MJJAS surface soil moisture ($10\,cm$) from a) FBC-1989 and b) FBC-1983 experiments. Thin black lines are for each perpetual year and thick red curves represent the 95% significance level.

Figure 9. JJAS averaged wind (vector) and magnitude (shaded) in ms^{-1}. Wind at 850 hPa from a) control simulation, b) sensitivity experiment and c) sensitivity minus control experiment. Wind at 200 hPa from d) control simulation, e) sensitivity experiment and f) sensitivity minus control experiment. Blue contour in (c) and (f) represent the 95% significance level.

Figure 10. Variance of 10-90 days filtered JJAS rainfall (mm^2day^{-2}) in a) control simulation (X_c), b) sensitivity experiment (X_s), c) percentage of change ($\frac{X_s-X_c}{X_c} \times 100$). Variance of 10-90 days filtered wind speed (m^2s^{-2}) in d) control simulation (V_c), e) sensitivity experiment (V_s), f) percentage of change ($\frac{V_s-V_c}{V_c} \times 100$).

Figure 11. Vertically integrated (surface-300 hPa) moisture convergence in a) control simulation, b) sensitivity minus control. Vectors represent the divergent part of wind ($q\vec{V}$) in $kg\,m^{-1}s^{-1}$ and shaded color represent the velocity potential ($\times 10^6\,kg\,m^{-1}s^{-1}$). Blue contour shows the significance at 95% level.

Figure 12. Composite of precipitation minus surface evaporation (P-E in $mm\,day^{-1}$) from a) control active phases, c) control break phases. Sensitivity minus control P-E composite from b) active phases, d) break phases. Blue contours shows the significance at 90% level. Composite of surface evaporation (in $mm\,day^{-1}$) from e) control active phases, g) control break phases. Sensitivity minus control evaporation for f) active composite, h) break composite.

Figure 13. Sensitivity minus control composite of wind at 850 hPa (in ms^{-1}) during a) strong active phase and b) strong break phase. Shaded color represents the amplitude of wind and blue contours show the regions significance at 95% level.

Figure 14. Vertically integrated (surface-300 hPa) moisture convergence a) active composite of control simulation, c) break composite of control simulation, b) sensitivity minus control of active composite and d) sensitivity minus control of break composite. Vectors represent the divergent part of wind ($q\vec{V}$) in $kg\,m^{-1}s^{-1}$ and shaded color represent the velocity potential ($\times 10^6\,kg\,m^{-1}s^{-1}$). Blue contour shows the significance at 95% level.

Figure 15. Moist static energy (in $kJ\,kg^{-1}$) averaged from surface to 700 hPa. MSE composite from control during a) strong active phase, c) strong break phase. Sensitivity minus control composite during b) strong active phase d) strong break phase. Stippled area indicates difference significant at 95% level.

Figure 16. Active (red) and break (black) composite of CI averaged equivalent potential temperature (θ_e in K) and vertical gradient of equivalent potential temperature ($\frac{d\theta_e}{dz}$ in $^\circ$C km^{-1}). a) θ_e from Control simulation, b) $\frac{d\theta_e}{dz}$ from control simulation, d) sensitivity minus control $\frac{d\theta_e}{dz}$.

Figure 17. Power spectra of CI averaged JJAS rainfall using 27 years of a) control simulation and b) sensitivity experiment. Red and blue lines represent the 95% and 5% significance level. Circles/ovals are indicating the frequency band where most of the changes took place.

Table 1. Experimental setup.

Experiment Name	Boundary Conditions (year)	Soil Moisture	Years of Model Run	Domain Size Lon × Lat
FBC-83	1983	Interactive	31	$76.1^\circ \times 58.5^\circ$
FBC-89	1989	Interactive	31	$76.1^\circ \times 58.5^\circ$
Control	1981-2008	Interactive	27	$76.1^\circ \times 58.5^\circ$
Sensitivity	1981-2008	Prescribed	27	$76.1^\circ \times 58.5^\circ$
Con-BD	1981-1989	Interactive	8	$101.9^\circ \times 81.32^\circ$
Sen-BD	1981-1989	Prescribed	8	$101.9^\circ \times 81.32^\circ$

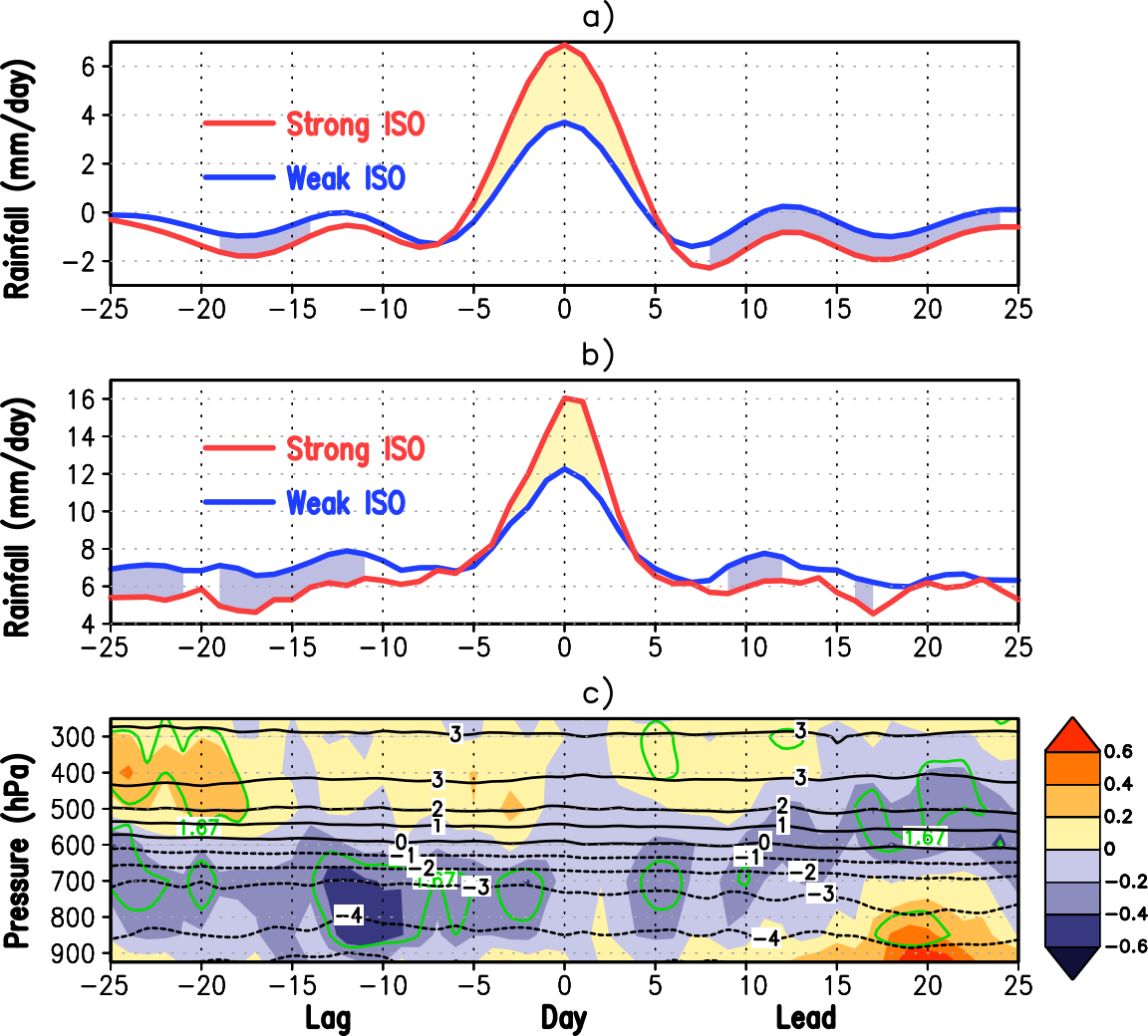
a)
Rainfall (mm/day)
Strong ISO
Weak ISO
b)
Rainfall (mm/day)
Strong ISO
Weak ISO
c)
Pressure (hPa)
Lag
Day
Lead

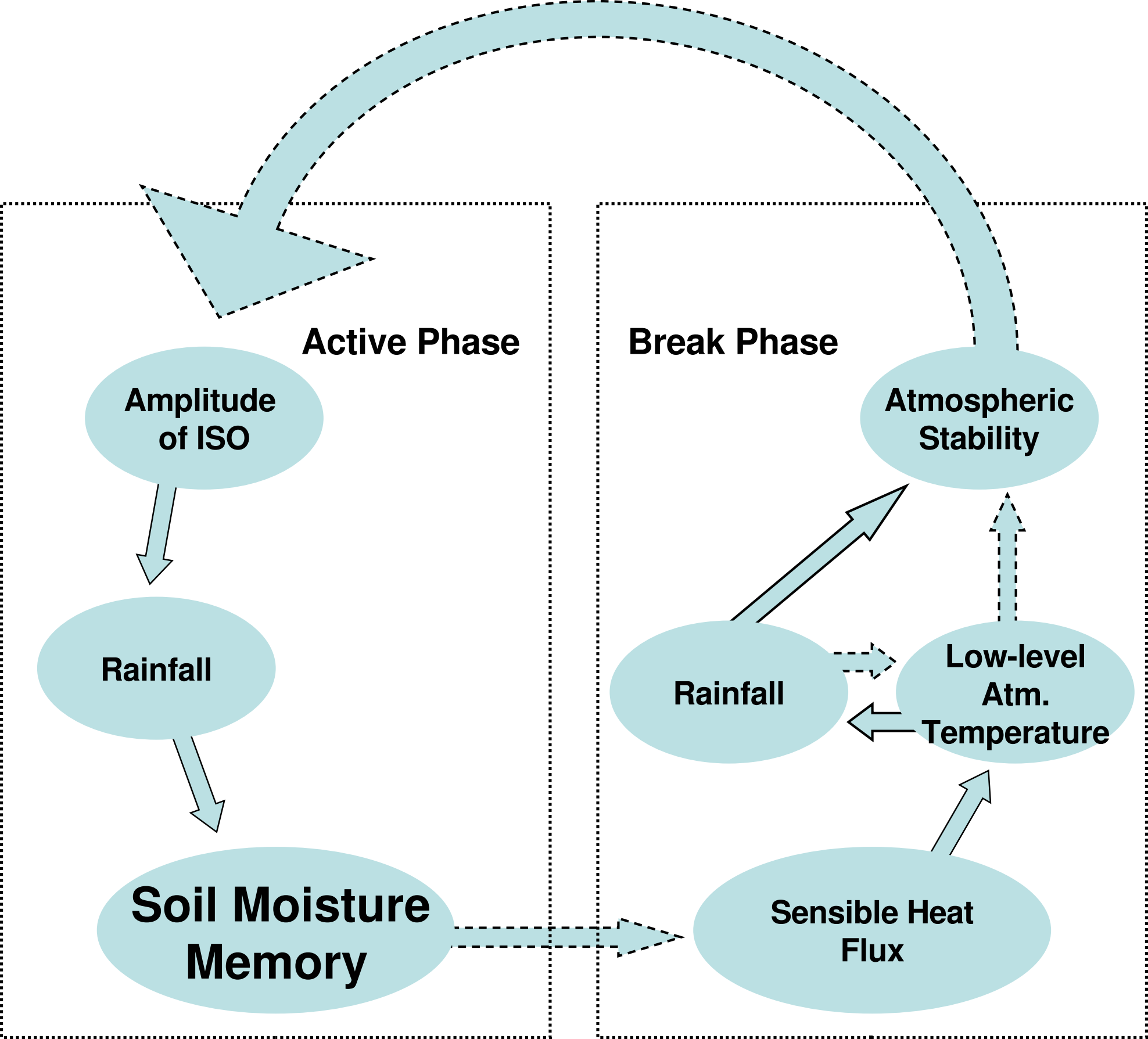
Active Phase
Break Phase
Amplitude of ISO
Rainfall
Soil Moisture Memory
Atmospheric Stability
Rainfall
Low-level Atm. Temperature
Sensible Heat Flux

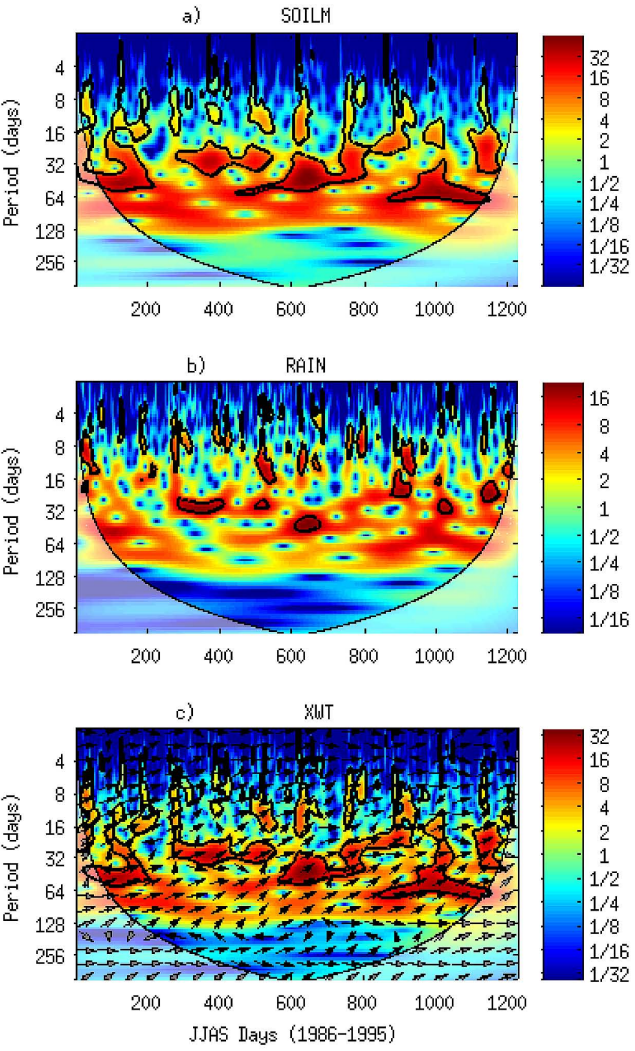
a) SOILM
b) RAIN
c) XWT
Period (days)
4
8
16
32
64
128
256
200
400
600
800
1000
1200
JJAS Days (1986-1995)
32
16
8
4
2
1
1/2
1/4
1/8
1/16
1/32

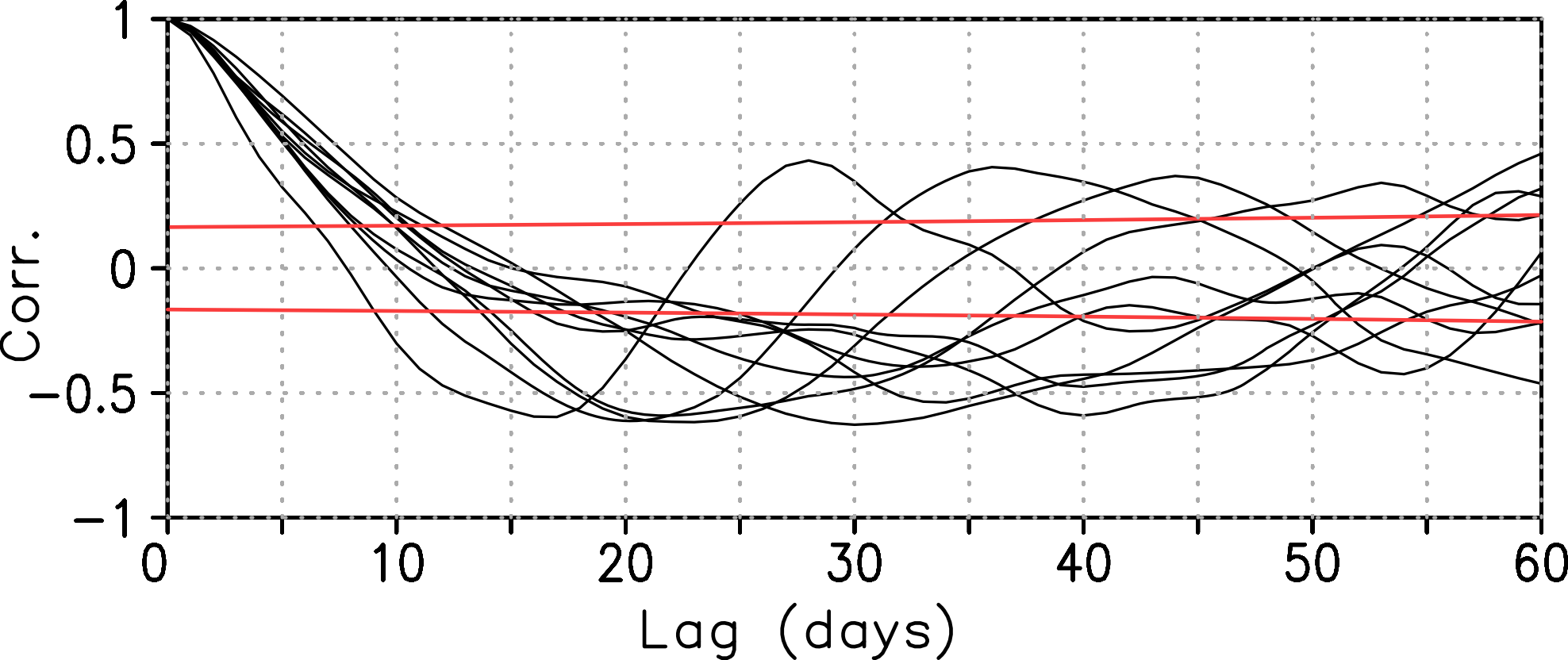
1
0.5
0
−0.5
−1
Corr.
0
10
20
30
40
50
60
Lag (days)

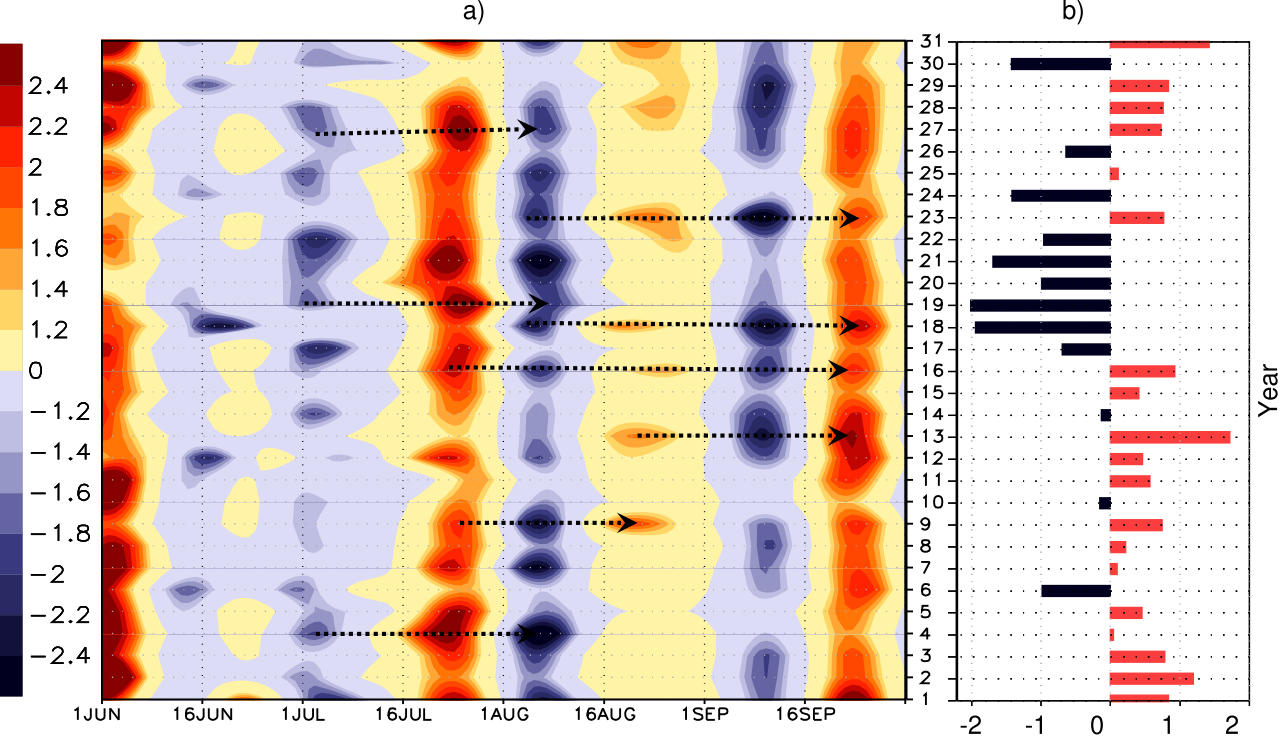

FBC-1989: mean = 83.82 cm, Interannual s.d. = 2.59 cm

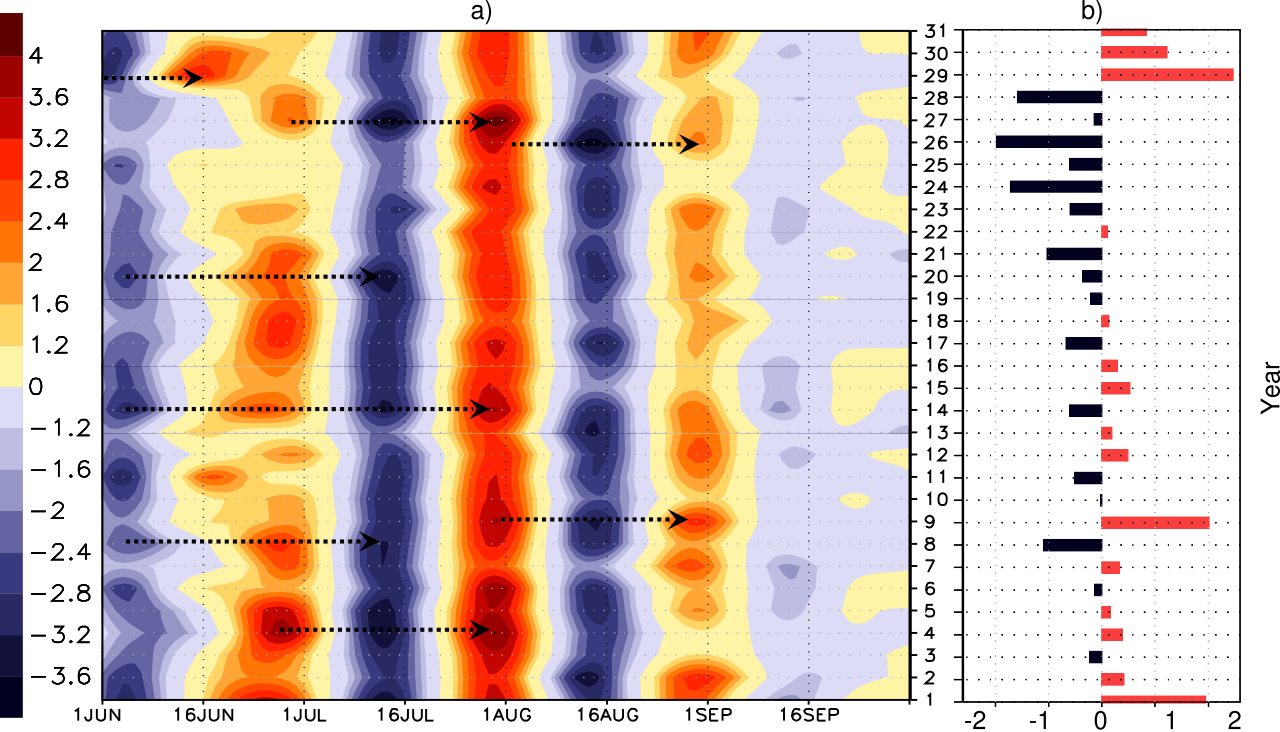

FBC-1983: mean = 88.55 cm, Interannual s.d. = 2.49 cm

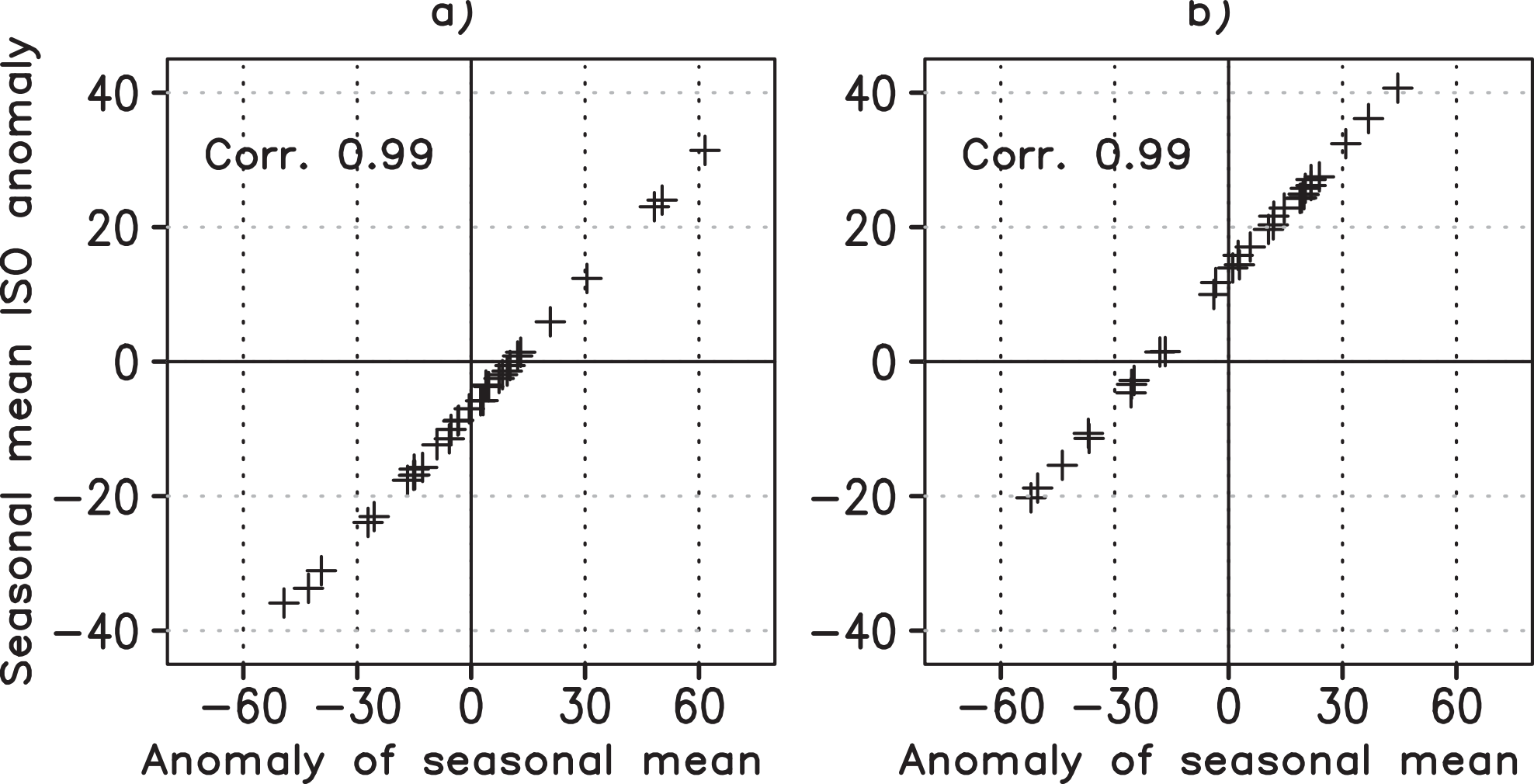
a)
b)
Corr. 0.99
Corr. 0.99
Seasonal mean ISO anomaly
Anomaly of seasonal mean
Anomaly of seasonal mean
40
20
0
−20
−40
−60
−30
0
30
60

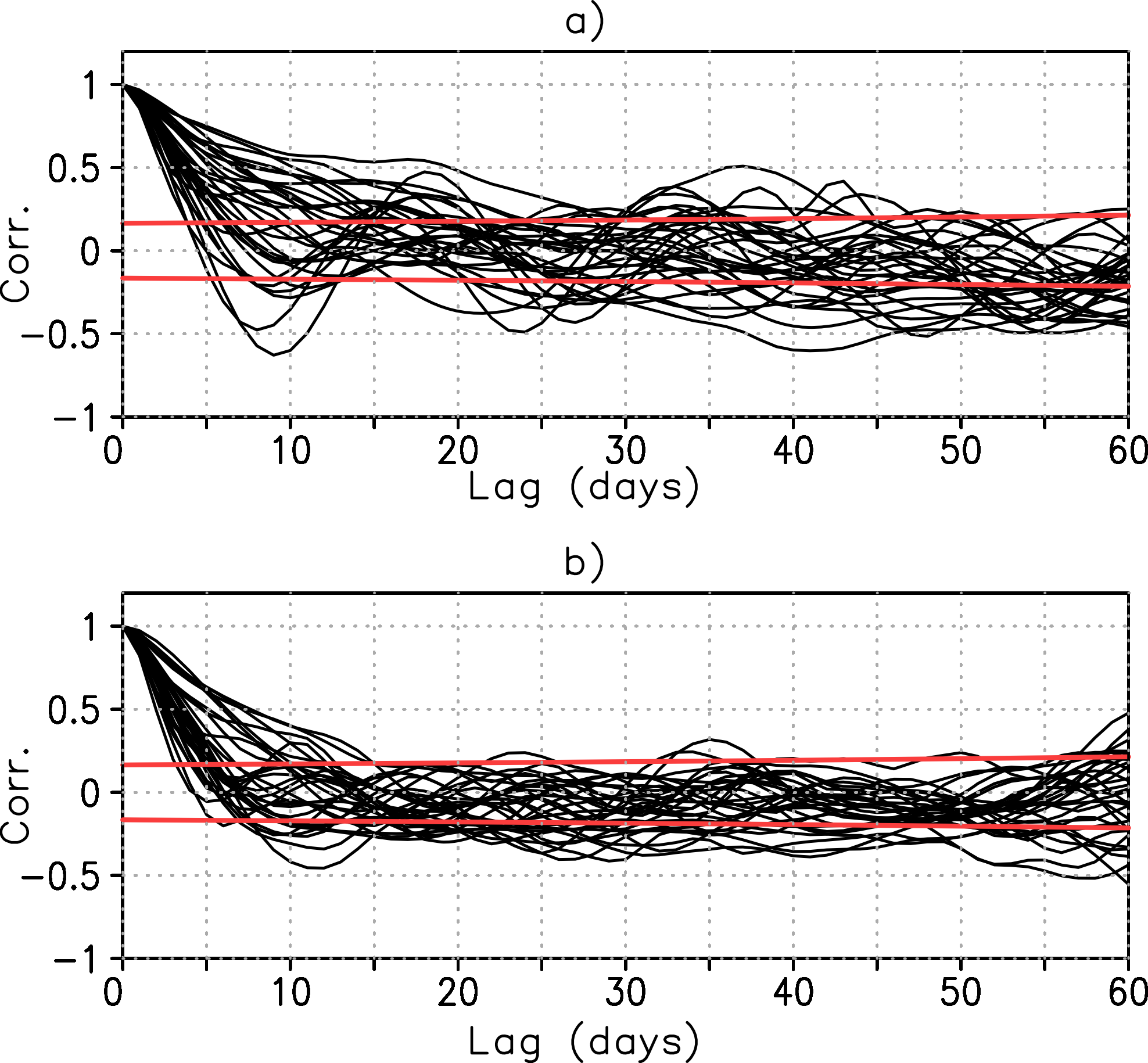
a)
Corr.
1
0.5
0
−0.5
−1
0
10
20
30
40
50
60
Lag (days)
b)
Corr.
1
0.5
0
−0.5
−1
0
10
20
30
40
50
60
Lag (days)

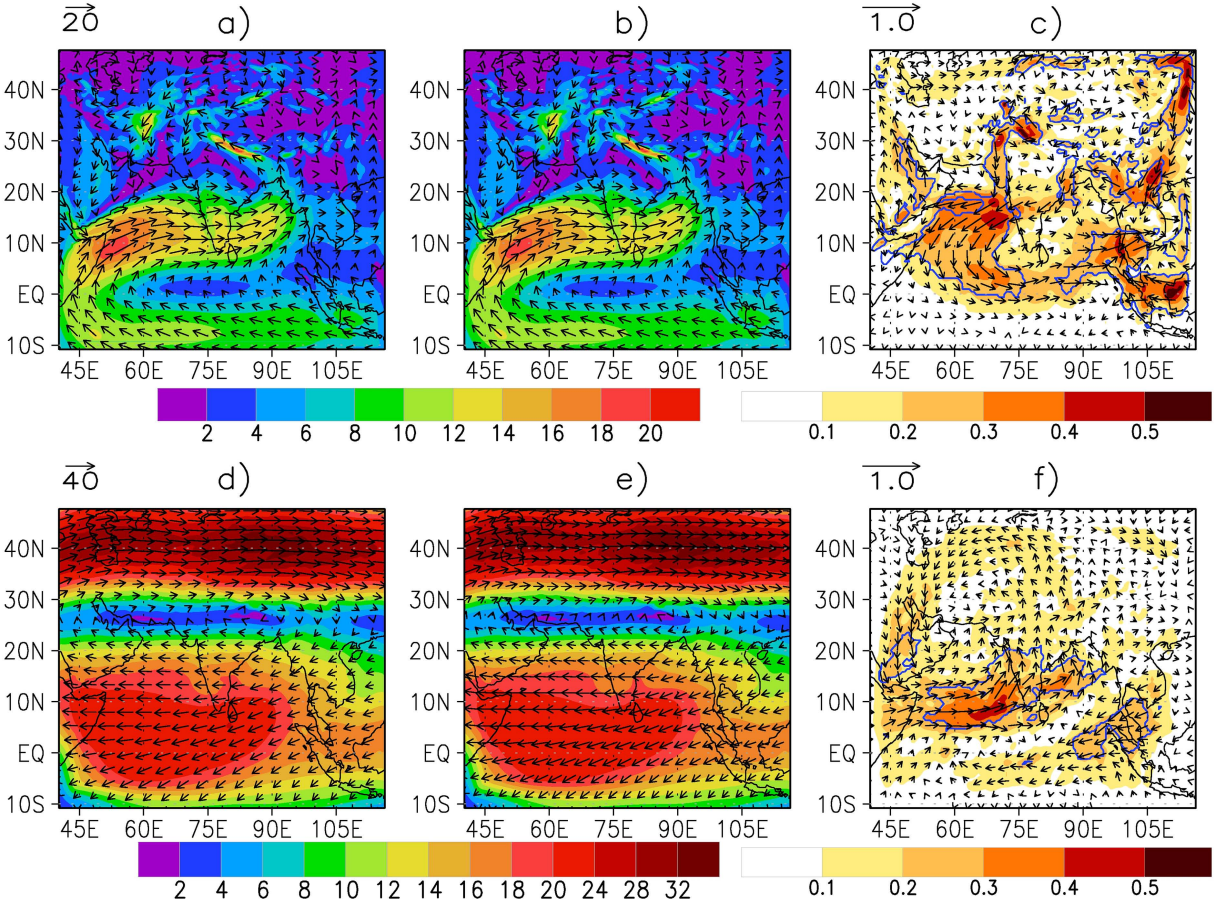
20
a)
b)
1.0
c)
40N
30N
20N
10N
EQ
10S
45E
60E
75E
90E
105E
2 4 6 8 10 12 14 16 18 20
0.1 0.2 0.3 0.4 0.5
40
d)
e)
1.0
f)
2 4 6 8 10 12 14 16 18 20 24 28 32
0.1 0.2 0.3 0.4 0.5

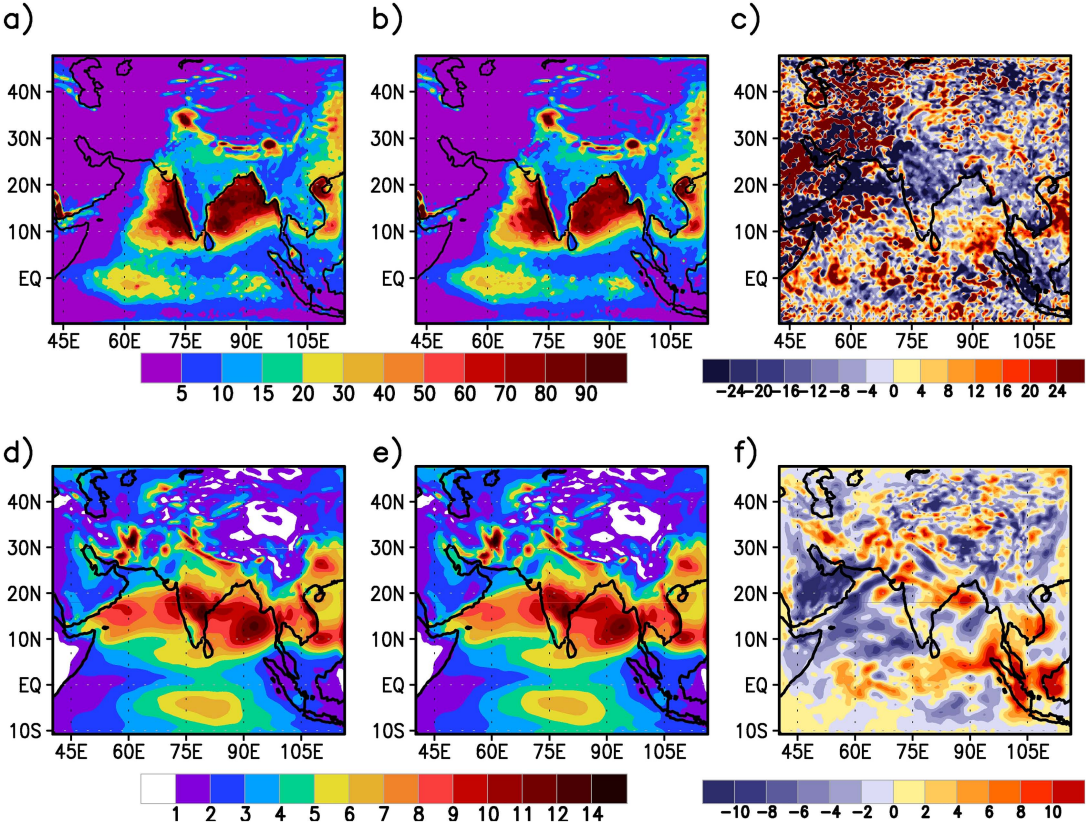
a)
b)
c)
d)
e)
f)
40N
30N
20N
10N
EQ
10S
45E
60E
75E
90E
105E
5 10 15 20 30 40 50 60 70 80 90
−24 −20 −16 −12 −8 −4 0 4 8 12 16 20 24
1 2 3 4 5 6 7 8 9 10 11 12 14
−10 −8 −6 −4 −2 0 2 4 6 8 10

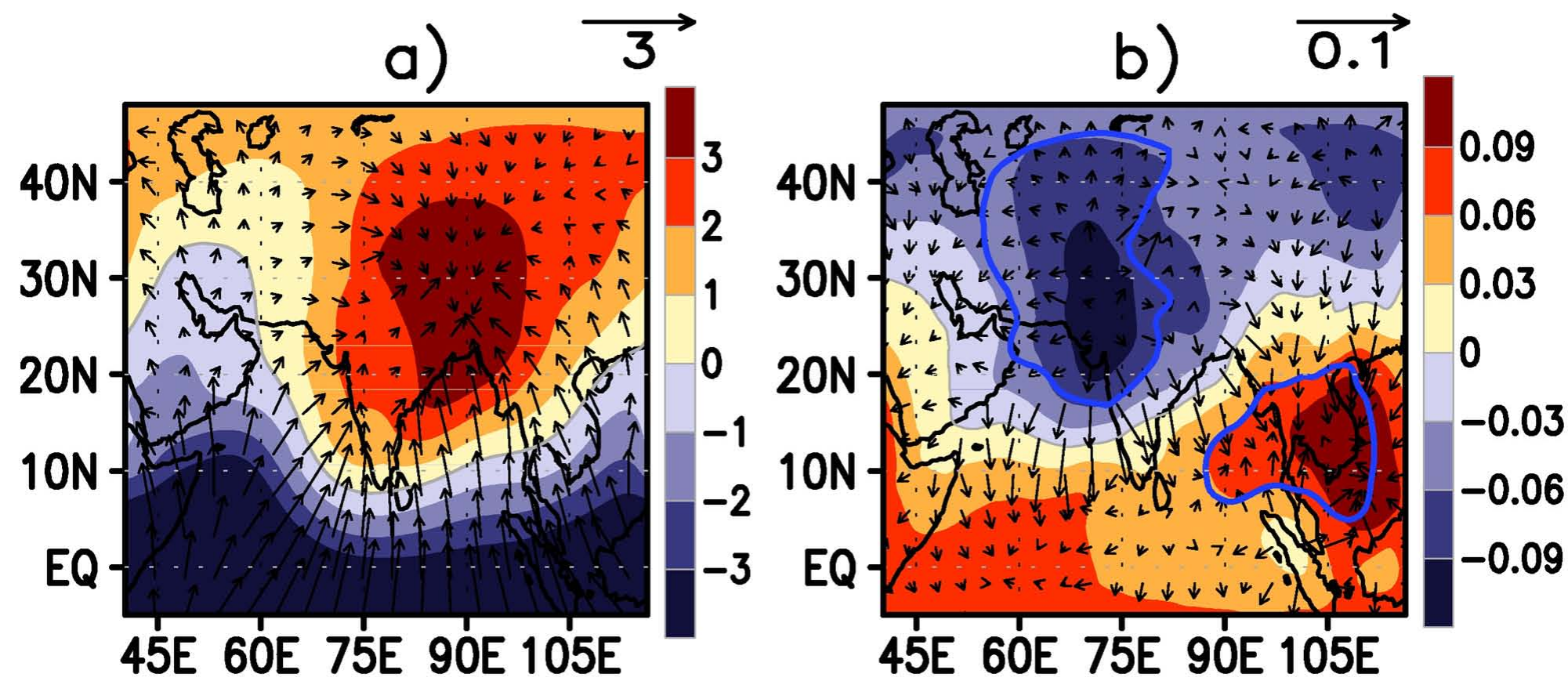
a)
3
40N
30N
20N
10N
EQ
45E
60E
75E
90E
105E
3
2
1
0
−1
−2
−3
b)
0.1
40N
30N
20N
10N
EQ
45E
60E
75E
90E
105E
0.09
0.06
0.03
0
−0.03
−0.06
−0.09

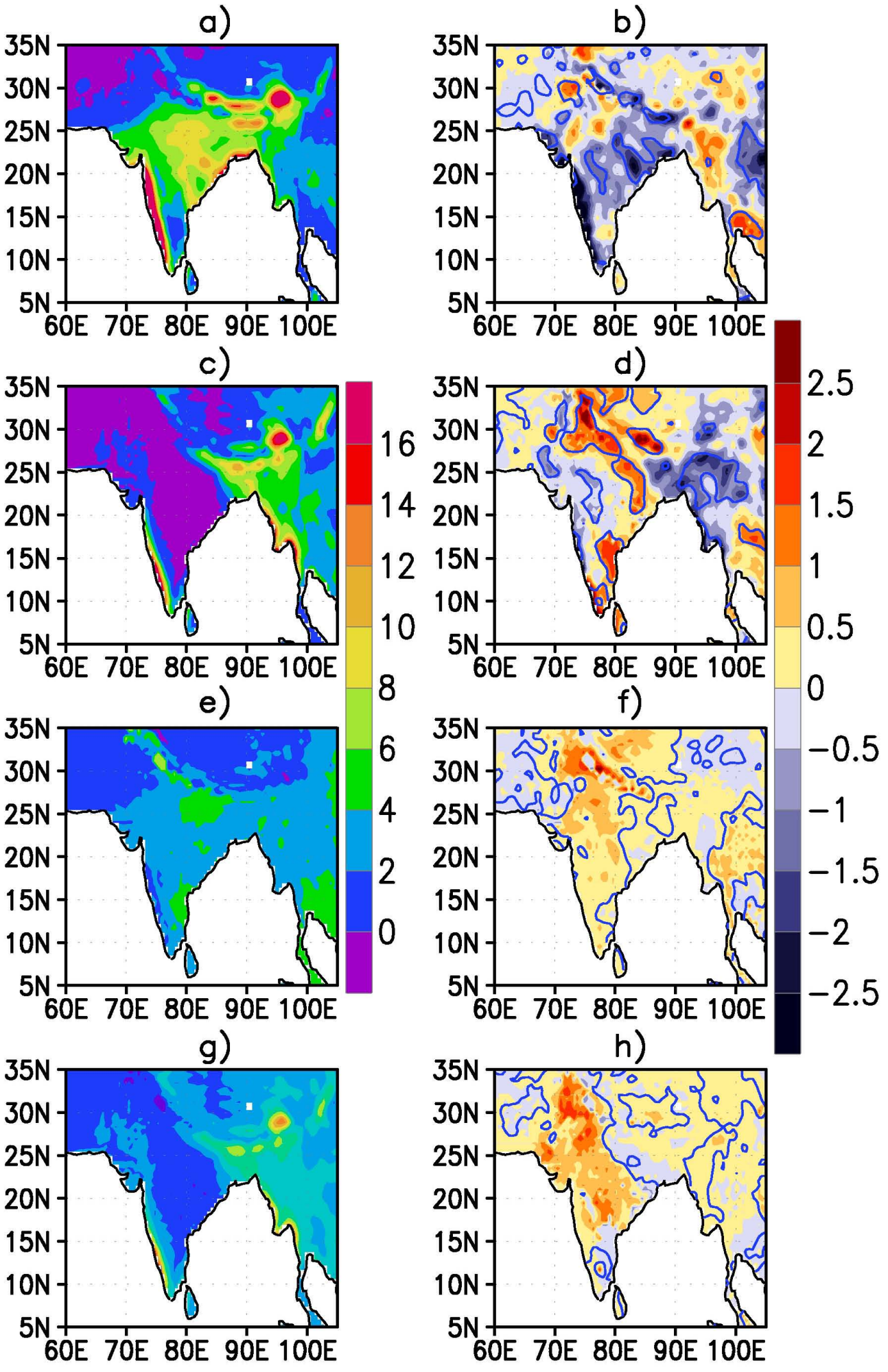
a)
b)
c)
d)
e)
f)
g)
h)
35N
30N
25N
20N
15N
10N
5N
60E 70E 80E 90E 100E
16
14
12
10
8
6
4
2
0
2.5
2
1.5
1
0.5
0
−0.5
−1
−1.5
−2
−2.5

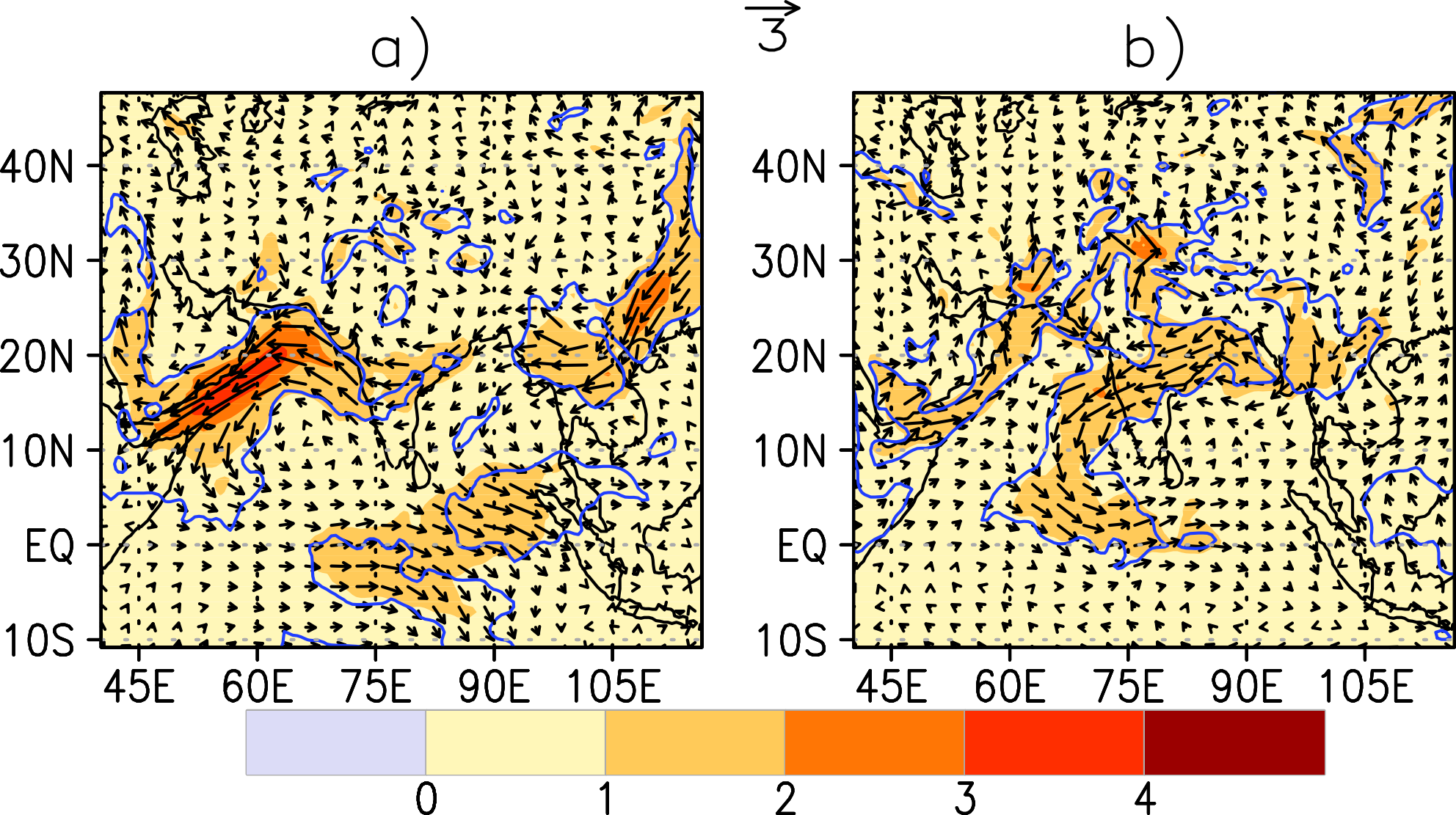
a)
b)
40N
30N
20N
10N
EQ
10S
45E
60E
75E
90E
105E
0
1
2
3
4

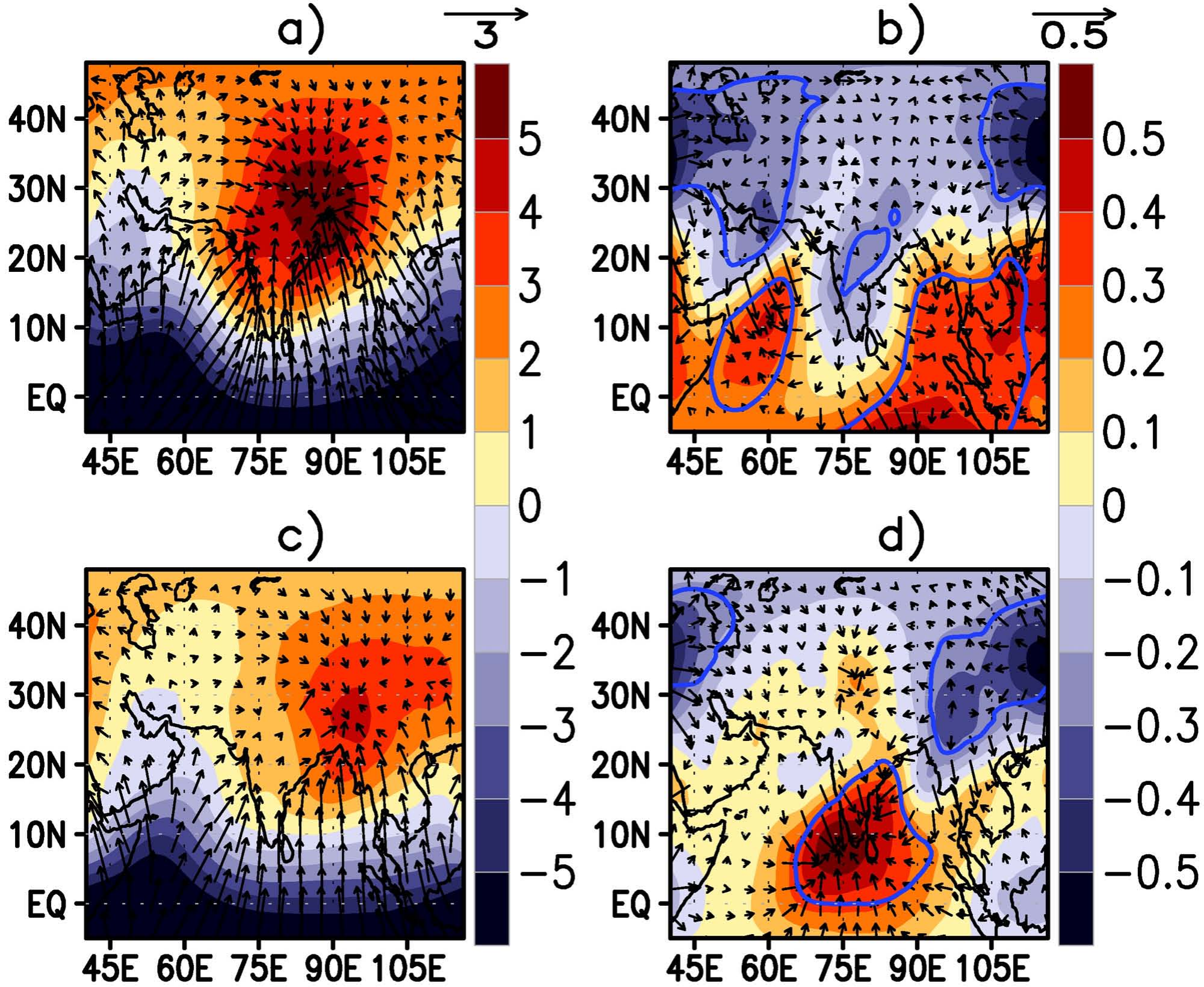
a)
3
40N
30N
20N
10N
EQ
45E 60E 75E 90E 105E
5
4
3
2
1
0
−1
−2
−3
−4
−5
b)
0.5
40N
30N
20N
10N
EQ
45E 60E 75E 90E 105E
0.5
0.4
0.3
0.2
0.1
0
−0.1
−0.2
−0.3
−0.4
−0.5
c)
40N
30N
20N
10N
EQ
45E 60E 75E 90E 105E
d)
40N
30N
20N
10N
EQ
45E 60E 75E 90E 105E

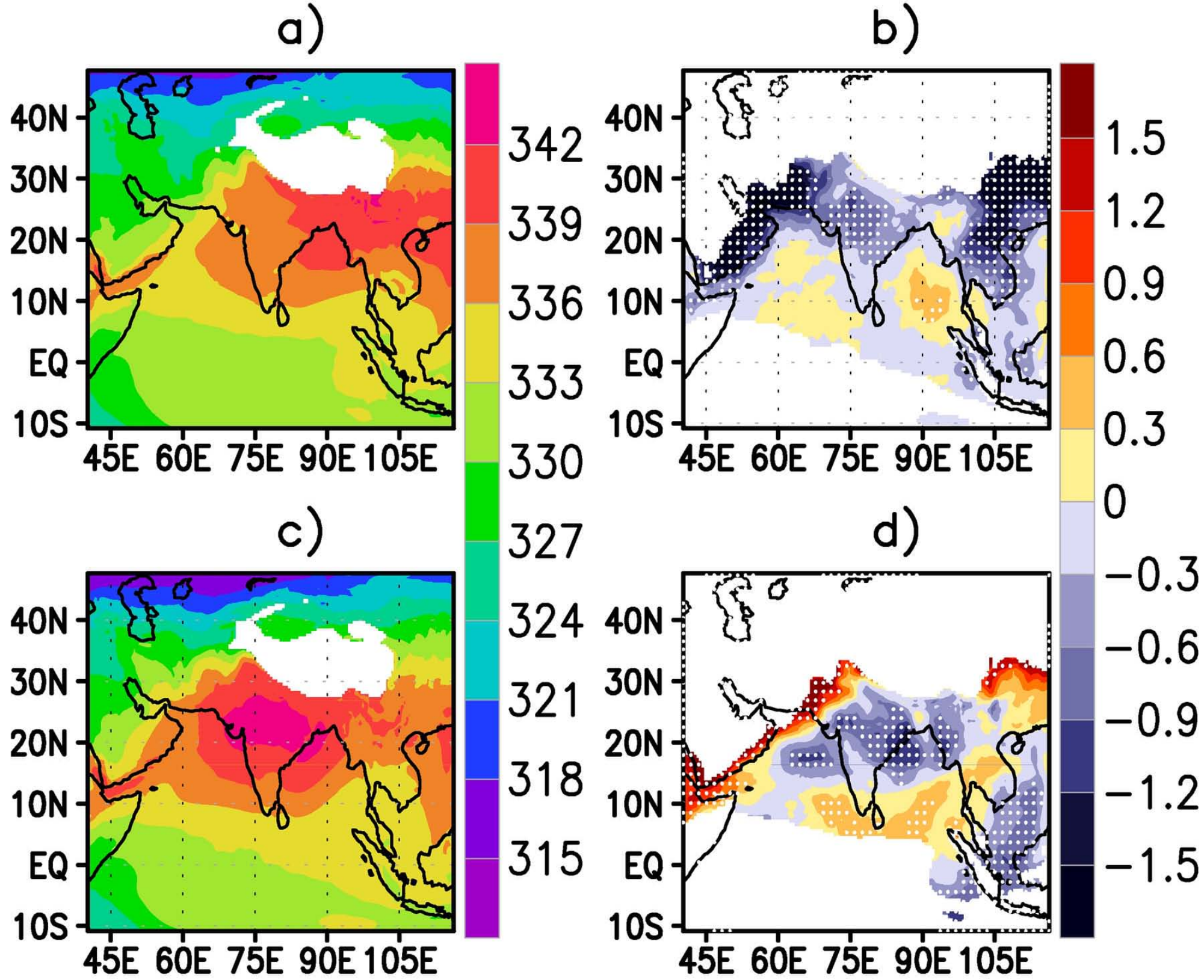
a)
b)
c)
d)
40N
30N
20N
10N
EQ
10S
45E
60E
75E
90E
105E
342
339
336
333
330
327
324
321
318
315
1.5
1.2
0.9
0.6
0.3
0
−0.3
−0.6
−0.9
−1.2
−1.5

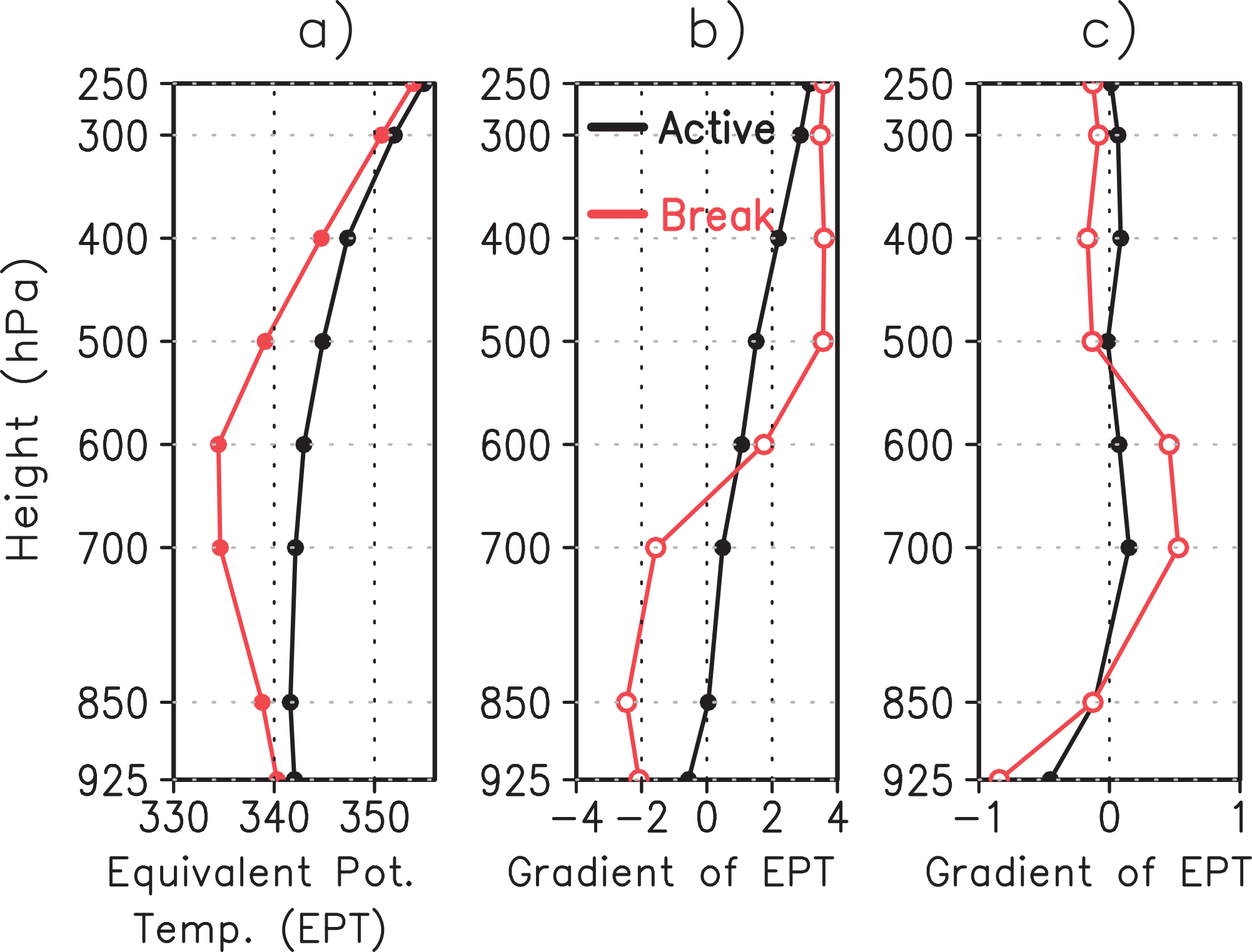
a)
b)
c)
Active
Break
Height (hPa)
250
300
400
500
600
700
850
925
330
340
350
−4
−2
0
2
4
−1
0
1
Equivalent Pot. Temp. (EPT)
Gradient of EPT
Gradient of EPT

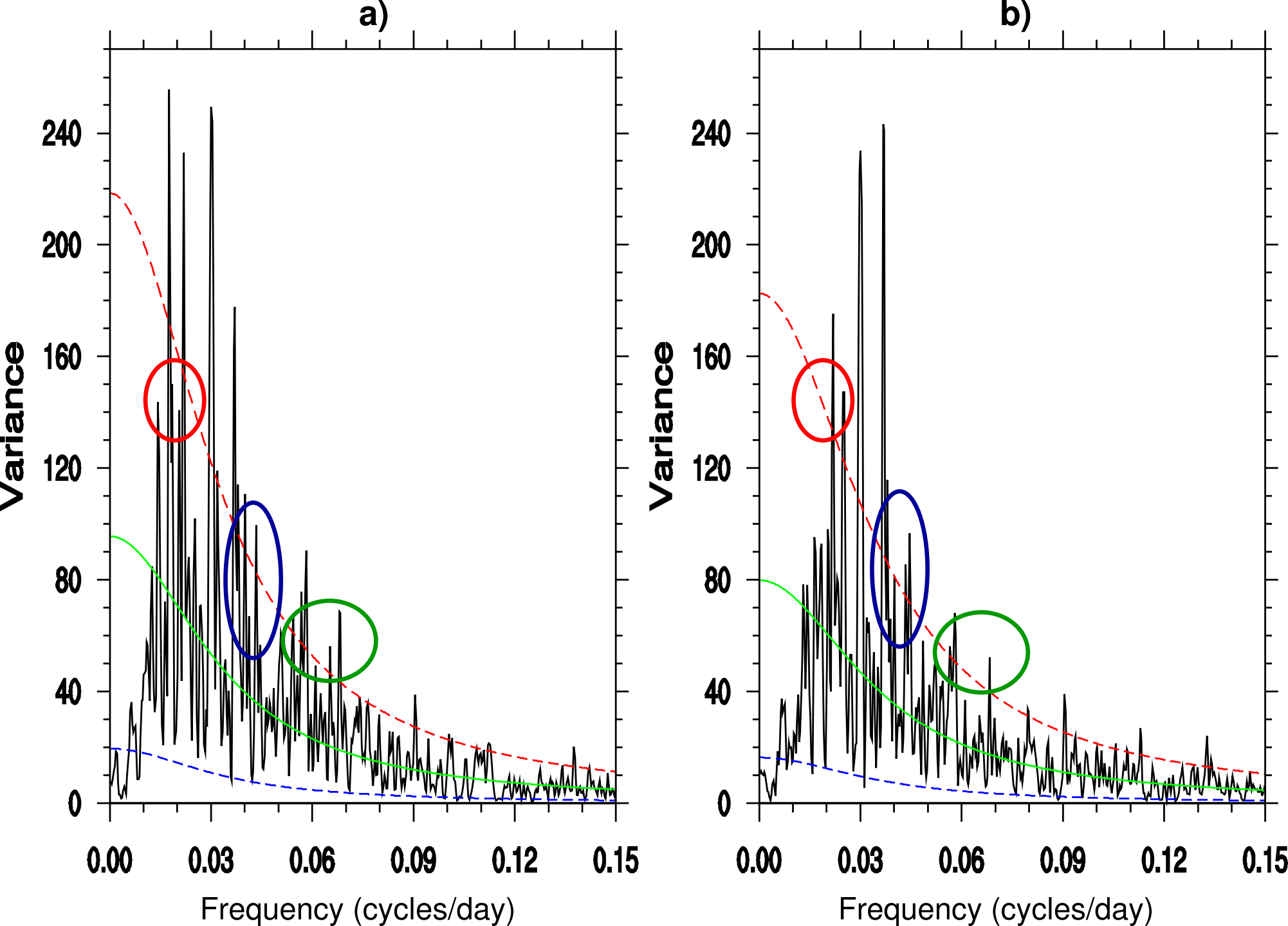
a)
b)
Variance
240
200
160
120
80
40
0
0.00
0.03
0.06
0.09
0.12
0.15
Frequency (cycles/day)